NUCLEAR SPIN-LATTICE RELAXATION OF SEVERAL NUCLEI IN ANTIFERROMAGNETIC $Rb_2MnCl_4 \cdot 2H_2O$

Thesis for the Degree of Ph. D.

MICHIGAN STATE UNIVERSITY

CHARLES EMERY TAYLOR

1967

This is to certify that the

thesis entitled

Nuclear Spin-Lattice Relaxation of Several Nuclei in Antiferromagnetic $Rb_2MnCl_4.2H_2O$

presented by

CHARLES EMERY TAYLOR

has been accepted towards fulfillment
of the requirements for

Ph.D. degree in Physics

J A Cowen
Major professor

Date Aug 2, 1967

ABSTRACT

NUCLEAR SPIN-LATTICE RELAXATION
OF SEVERAL NUCLEI IN
ANTIFERROMAGNETIC $Rb_2MnCl_4 \cdot 2H_2O$

by Charles Emery Taylor

Rubidium Manganese Chloride di-hydrate ($Rb_2MnCl_4 \cdot 2H_2O$) is a triclinic crystal which becomes antiferromagnetic below 2.24°K. Measurements of the nuclear spin-lattice relaxation time T_{1n} have been made as a function of temperature for four nuclei, Rb^{87}, Rb^{85}, Cl^{35}, and H^1, in the temperature range from 1.6°K to 0.45°K, and in one instance, for Rb^{87}, to 0.32°K. Standard rf pulse techniques were used, and the experiments were carried out in zero external magnetic field. The temperature dependence of T_{1n} was qualitatively the same for all four lines, and a least squares fit to the data for each line was made using a theory based on a two magnon Raman relaxation mechanism, which, in the small k approximation gives

$$T_{1n}^{-1} = 2K\int_{T_{AE}/T}^{\infty} x(e^x-1)^{-1}dx$$

The values of 2K and T_{AE} which give the best fit to

the data along with the frequencies of the measured lines at 1.1°K and the nuclear spin are given in the table for each nucleus.

Nucleus	Spin	Freq. (MHz) at 1.1°K	$2K(sec)^{-1}(°K)^{-3}$	$T_{AE}(°K)$
H^1	1/2	18.1	1.96×10^3	2.15
Cl^{35}	3/2	8.53	1.08×10^3	2.47
Rb^{87}	3/2	3.89	9.73×10^2	2.36
Rb^{85}	5/2	3.22	1.33×10^2	2.04

The value of 2K for protons is calculated from the theory and found to be too small be a factor of one to two orders of magnitude, suggesting that the small k approximation is not applicable in this case. An approximate theory, utilizing all k from 0 to k_m, is developed and used to calculate the proton T_{1n}. The result is in good agreement with experiment. The following conclusions are drawn: (1) relaxation occurs via an intrinsic two magnon Raman process and is not due to the presence of paramagnetic impurities, (2) the temperature dependence of T_{1n} is influenced by a large energy gap in the magnon spectrum, (3) the influence of the quadrupole moment on the temperature dependence of T_{1n} is small, and (4) the use of the small k approximation is not consistent with the presence of a large energy gap in the magnon spectrum.

NUCLEAR SPIN-LATTICE RELAXATION OF SEVERAL NUCLEI IN ANTIFERROMAGNETIC $Rb_2MnCl_4 \cdot 2H_2O$

By

Charles Emery Taylor

A THESIS

Submitted to
Michigan State University
in partial fulfillment of the requirements
for the degree of

DOCTOR OF PHILOSOPHY

Department of Physics

1967

DEDICATION

This thesis is dedicated to my father and mother.

ACKNOWLEDGMENTS

The author wishes to acknowledge the support and guidance of Dr. J. A. Cowen, whose enthusiasm, sense of humor and dedication have made the last three years both enjoyable and worthwhile. He also offers his thanks to Dr. R. D. Spence for several helpful discussions concerning this thesis and for bearing without complaint the burden of a sometimes noisy research group on his premises; to Dr. E. H. Carlson for several suggestions concerning the electronic apparatus and for the time and effort which he gave en route to 0.32°K; to Dr. George T. Johnston III for the computer work involved in this thesis and for his friendship during the last three years; to the machine and electronics shop for their general good humor and craftsmanship, and to the National Science Foundation for their support of this project.

TABLE OF CONTENTS

LIST OF TABLES

LIST OF FIGURES

LIST OF APPENDICES

I. INTRODUCTION

The nuclear spin-lattice relaxation time of nuclei in antiferromagnetically ordered materials was first measured by Hardeman and Poulis in 1956.[1] The relaxation was found to result primarily from the magnetic interaction between the nuclei and the exchange-coupled electron spin system.[2] At temperatures low enough that the latter can be represented mathematically by the spin wave approximation,[3] the dominant relaxation process can be described as inelastic scattering of spin waves by the magnetic dipole field of the nucleus,[4] with an associated nuclear spin flip. Thus the relaxation mechanism depends on the spin-wave or magnon population, which is strongly temperature dependent. Existing theories of the relaxation process can therefore be judged by comparing the predicted temperature dependence of T_{1n} with that obtained experimentally.

It has been the purpose of the work described in this thesis, (1) to construct a reasonably inexpensive apparatus capable of measuring T_{1n} from 4.2°K to 0.45°K over a frequency range from 3 to 20 MHz, (2) to use this apparatus to measure T_{1n} as a function of temperature for a number of nuclear species (H^1, Cl^{35}, Rb^{87} and Rb^{85}) in

antiferromagnetic single crystals of $Rb_2MnCl_4 \cdot 2H_2O$ and (3) to compare the results with those predicted by magnon relaxation theory.

Background

Nuclear Magnetization. Nuclear spins in an antiferromagnet see a strong magnetic field produced by the ordered electron spins. The static Hamiltonian for a given nuclear spin is[5]

$$\mathcal{H}_N = -\underline{\mu} \cdot \underline{H} = -\gamma_N \hbar \underline{I} \cdot \underline{H} \qquad (1.1)$$

where μ is the magnetic moment of the nucleus, γ_N is the nuclear gyromagnetic ratio, $\underline{I}$ is the dimensionless angular momentum operator, and $\underline{H}$ is the average local field at the nucleus due to the electron spins. We have neglected the nuclear dipole-dipole interaction because it is small compared to the interaction between the nucleus and the electron and have chosen a nucleus whose quadrupole moment is zero.

If we choose a coordinate system for which $\underline{H}$ is in the z-direction, $\underline{H} = \hat{k}H$, and

$$\mathcal{H}_N = -\gamma_N \hbar H I_z \qquad (1.2)$$

The allowed energies of the nuclear spin, given by the eigenvalues of $\mathcal{H}_N$, are

$$E_m = -\gamma_N \hbar H m \qquad m = I, I-1, \ldots -I \qquad (1.3)$$

where m represents the eigenvalues of I_z. The energy difference between adjacent states is therefore $\Delta E = \hbar\gamma_N H = \hbar\omega_L$, where ω_L is the classical Larmor precession frequency, or resonant frequency, of the system.

Because the energy of the nuclear spin is quantized, the magnetic moment cannot assume an arbitrary orientation with respect to the magnetic field, but can take up only those orientations for which the z-component of the angular momentum is given by $J_z = \hbar m$.

In discussing the methods for measuring T_{1n}, we will be interested in the total nuclear magnetization $\underline{M}$ of the sample, given by

$$\underline{M} = \sum_k \underline{\mu}_k \qquad (1.4)$$

where $\underline{\mu}_k$ is the magnetic moment of the k^{th} nucleus and the index k runs from 1 to N, the total number of nuclei. In thermal equilibrium, the expectation value of the total nuclear magnetization must be parallel to the magnetic field,[6] $\underline{H}$, so that the x- and y-components of $\underline{M}$ are zero. To find the z-component of the magnetic moment, it is necessary to determine the relative populations of the Zeeman levels. For simplicity, consider a system of nuclei with spin I = 1/2. At thermal equilibrium, the populations of the Zeeman levels are proportional to the Boltzmann factor $\exp(-E_m/k_B T)$ where T is the absolute temperature

of the lattice.[7] Let N^+ and N^- represent the populations of the ground and excited states respectively. The ratio of N^+ to N^- is then

$$\frac{N^+}{N^-} = e^{\gamma_N \hbar H/k_B T} \tag{1.5}$$

which is greater than one. There are therefore more spins with m = +1/2 than with m = -1/2 and as a result there is a net nuclear magnetization in the z-direction given by

$$M_z = \sum_k \mu_{kz} = (N^+ - N^-)\frac{\gamma_N \hbar}{2} = \frac{\gamma_N \hbar}{2}(N^-)(e^{\frac{\gamma_N \hbar H}{k_B T}} - 1) \tag{1.6}$$

In general $k_B T$ is much greater than $\gamma_N \hbar H$. Assuming that this is the case, from equation (1.5) we have $N^+ \simeq N^-$ so that $N^- \simeq N/2$ where N is the total number of nuclei. Similarly expanding the exponential in equation (1.6) and using $N^- = N/2$ gives

$$M_z = \frac{N\gamma^2 \hbar^2 H}{4k_B T} \tag{1.7}$$

If the nucleus has an electric quadrupole moment, the situation is not as simple. The gradient of the crystalline electric field partially removes the degeneracy of the nuclear energy levels.[8] The internal magnetic field produces Zeeman splitting of the remaining degenerate levels. Although the energy levels are no longer necessarily equally spaced, the populations are still proportional to the Boltzmann factor, and at thermal

equilibrium there exists a nuclear magnetization $\underline{M}$ which is parallel to $\underline{H}$.

Nuclear Spin-Lattice Relaxation. If a non-equilibrium distribution of the spins is produced, for example by an rf pulse at the resonant frequency, the system will relax back to the equilibrium distribution in a time characterized by the nuclear spin-lattice relaxation time, T_{1n}. The subscript n has been added to emphasize that we are considering nuclear as opposed to electron spin relaxation processes. By T_{1n} we mean the time constant associated with the exponential recovery of the z-component of the magnetization[9] from a non-equilibrium situation.

T_{1n} is a good measure of the strength of the interactions between a nuclear spin and the lattice, since it is these interactions which provide the relaxation mechanism. The term "lattice" is used loosely here, and would be more properly replaced by the word "surroundings." In antiferromagnets, for example, the nuclei relax to the electron spin system which eventually gives the energy thus absorbed to the lattice in the form of phonons. Examples of possible interactions[10] leading to spin-lattice relaxation in solids are (1) the magnetic interaction between the nuclei and paramagnetic impurities, (2) the interaction between the nuclear quadrupole moment and the gradient of the crystalline electric field, (3) the changing magnetic field at the nuclear site due

to phonon-induced fluctuations of the electron spin system and (4) the changing magnetic field at the nuclear site due to exchange-induced fluctuation of the ordered-electron spin system. Of these the last is generally the dominant mechanism in the temperature range studied. The effect of paramagnetic impurities will be discussed in Chapter V, but it is evidently much smaller than the dominant mechanism in our case. The second and third examples both depend on the phonon population which is negligible for temperatures very small compared to the DeBye temperature.[11] We are left with the effect of the interaction between the nuclei and the exchange-coupled electron spin system. The low energy thermal excitations of this system are called magnons. The nucleus relaxes to the magnon system, and the energy thus absorbed is eventually transferred to the lattice, but in quanta which are generally much larger than the nuclear quanta,[12] so that the nuclear relaxation will be independent of the relaxation time of the atomic spins.

II. MEASUREMENT METHODS

Measurements of T_{1n}, the nuclear spin-lattice relaxation time, were made in zero external magnetic field using standard radio frequency (rf) pulse techniques to be described below. These techniques depend on the detection of free induction decay (FID) signals and spin echoes. This chapter will present a brief discussion of these phenomena.

Theory

The theory of spin echoes and free induction decay is well known.[13,14,15] The brief discussion given in this chapter can be supplemented by the above references.

For simplicity, consider a system of spin 1/2 nuclei in a magnetic field $\underline{H}$ directed along the z-axis. If the system is in thermal equilibrium, at time t = 0, the populations of the two Zeeman energy levels will be proportional to the Boltzmann factor, leading to a net magnetization parallel to $\underline{H}$ of magnitude $M_z(0) = M_o$, given by Eq. (1.7) as discussed in Chapter I. In equilibrium no net magnetization perpendicular to $\underline{H}$ exists. However, a circularly polarized magnetic field $\underline{H}_1$, of frequency ω_L, applied to the system in the form

of an rf pulse will produce a non-equilibrium situation in which a transverse magnetization $M_\perp$ does exist. As will be shown, the precession of $M_\perp$ can be detected and the amplitude of the detected signal can be used under certain circumstances to measure the spin-lattice relaxation time T_{1n}.

A classical description of the phenomena of spin echoes and free induction decay leads to the same equations as the quantum mechanical theory, and has the advantage that it is easily visualized, so it will be used here. In Figure 2.1A, the net magnetization $\underline{M}_o$ is shown parallel to $\underline{H}$. A magnetic field $\underline{H}_1$, perpendicular to $\underline{H}$ and rotating at the Larmor frequency, exerts a torque $\underline{M}_o \times \underline{H}_1$ on $\underline{M}_o$, causing $\underline{M}_o$ to precess about $\underline{H}_1$ with angular frequency $\omega_1 = \gamma_N H_1$. When the angle θ between $\underline{M}_o$ and $\underline{H}$ becomes non-zero, the torque $\underline{M}_o \times \underline{H}$ will cause $\underline{M}_o$ to precess about $\underline{H}$ at the Larmor frequency. In order to eliminate the visual confusion which this introduces, Figures 2.1B through 2.1F are drawn in a coordinate system (x', y', z') rotating about the z-axis at frequency $\Omega = -\hat{k}\gamma_N H$. In the rotating frame the magnetization sees an effective field,[16] in this case equal to $\underline{H}_1$, which is constant in time. $\underline{H}_1$ has been chosen to lie in the x'-direction. If $\underline{H}_1$ is removed after a time $t_\theta = t_{\pi/2} = \frac{\pi}{2\omega_1}$, the net magnetization will be in the x'-y' plane, and $M_z(t_{\pi/2})$ will be zero (Fig. 2.1C). Such

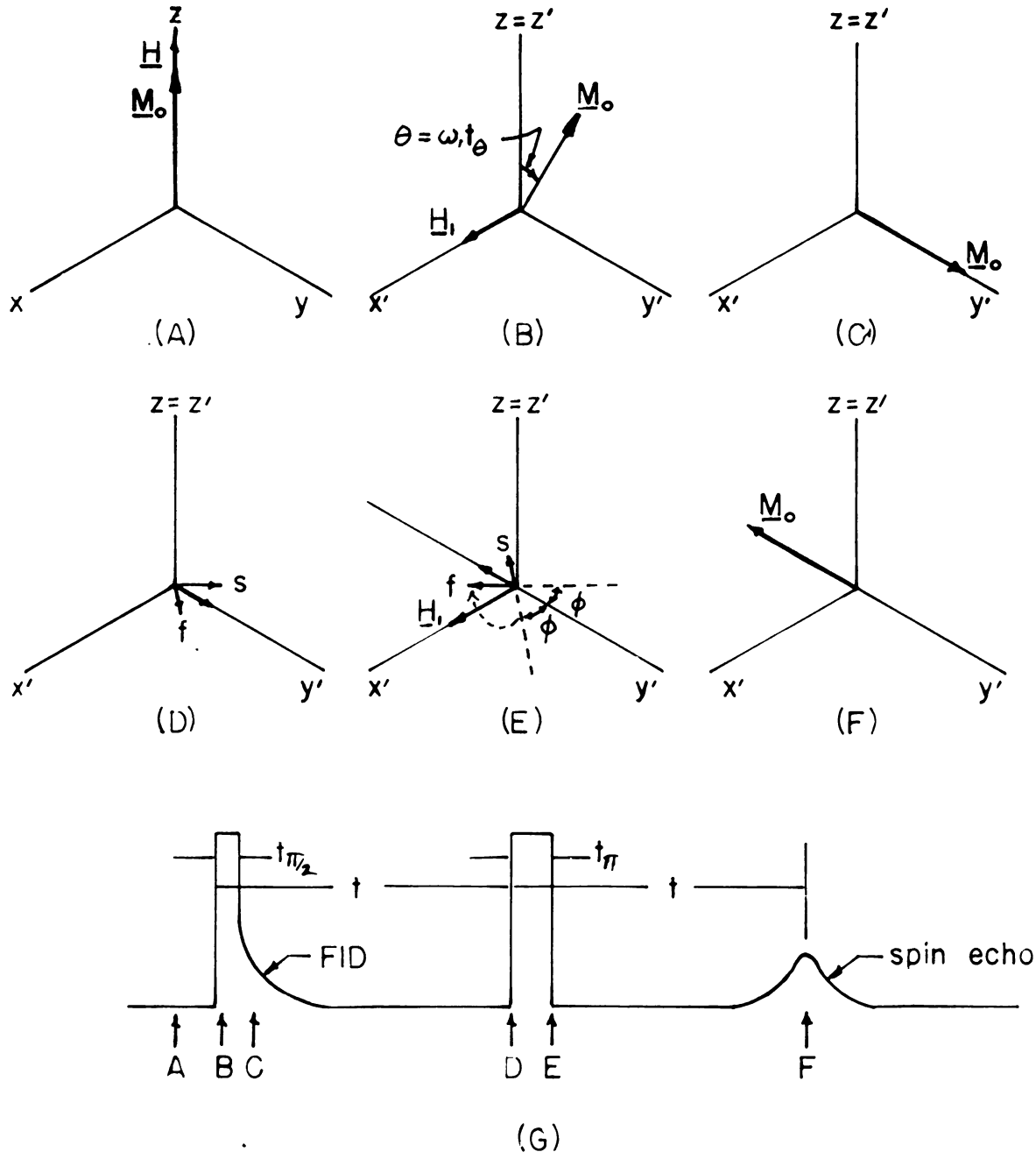

Fig. 2.1. Formation of free induction decay and spin echo signals.

a pulse of $\underline{H}_1$ is called a 90° pulse because it causes $\underline{M}_o$ to precess 90° around $\underline{H}_1$. When $\underline{H}_1$ is removed, $\underline{M}$ will remain stationary in the rotating reference frame and hence will precess at frequency ω_L in the lab system. This precessing magnetization will induce an emf in a coil whose axis is in the x-y plane. The magnitude of the emf induced will be proportional to the magnitude of the net component of $\underline{M}$ in the x-y plane, which in turn depends initially on the magnitude of the z-component of $\underline{M}$ that existed just before the pulse was applied. This is shown in Appendix A.

In the experiments for this thesis, the magnetic field $\underline{H}$ was the local magnetic field in the crystal, resulting from the antiferromagnetically ordered electron spins. Due to local field inhomogeneities, the local field has different values for different crystallographically equivalent spins leading to a spread in Larmor precession frequencies. Therefore, as viewed in the rotating frame, the magnetization fans out (Fig. 2.1D). As the spins get further out of phase, the net transverse magnetization goes to zero and the resulting signal also decays to zero. Such a signal is called a free induction decay tail or an FID.

It is possible to bring the spins back into coherence by the application of a second pulse of $\underline{H}_1$ a time t after the first pulse. For simplicity, we consider that $\underline{H}_1$ is again along the x'-axis and that its duration is such that $\underline{M}$ precesses through 180° around $\underline{H}_1$ (Fig. 2.1E).

The spins that had precessed ahead of the center of the distribution by an angle ϕ are now behind the center by the same angle. (These spins are labeled f in Figs. 2.1D and 2.1E.) Similarly those that lagged by ϕ (labeled s in Figs. 2.1D and 2.1E) are now ahead by ϕ. Therefore at a time 2t after the first pulse the spins will have regrouped (Fig. 2.1F) and will produce an emf in the receiver coil, which is called a spin echo. Figure 2.1G shows the pulses necessary for formation of an FID and a spin echo.

It should be noted that in general rf power is fed into the sample in the form of a linearly polarized rf pulse of frequency ω_L. This can be decomposed into two circularly polarized fields, one rotating at frequency ω_L in the same sense as the nuclear precession, and the other rotating at frequency ω_L in the opposite sense. The effect of the latter can be shown to be neglibible, and it is usually neglected. The H_1 discussed above is the circularly polarized component rotating in the same sense as the Larmor precession, and it is this component that produces the nuclear resonance.

Relaxation Effects

The above discussion has neglected the effects of relaxation phenomena. Application of a 90° pulse results in a non-equilibrium configuration of the spin

system. Through the mechanism discussed briefly in Chapter I, the spins are able to return to the equilibrium distribution, giving up their energy to the lattice. Thus the z-component of the nuclear magnetization grows from zero, right after the 90° pulse, to $\underline{M}_o$ after a sufficient length of time. The return to equilibrium is expressed by the equation

$$M_z(t) = M_o[1-\exp(-t/T_{1n})] \qquad (2.1)$$

which is derived in Appendix B. As explained earlier, the size of the FID after a 90° pulse is proportional to the magnitude of the z-component of $\underline{M}$ that existed just prior to the 90° pulse. It is therefore a measure of the degree to which the system has returned to equilibrium. The two pulse method for measuring T_{1n} takes advantage of this, and is discussed later in this chapter.

Relaxation to equilibrium also affects the amplitude of the spin echo. As the time t between the two echo forming pulses is increased, the amplitude of the echo decreases. This is usually due to mutual spin flips between neighboring nuclei which conserve energy but destroy the phase coherence of the transverse components of the nuclear magnetic moments. The resulting decay of the transverse magnetization can be described by an exponential with time constant T_{2n}, the spin-spin relaxation time. We assume throughout this discussion that $T_{1n} >> T_{2n}$. T_{2n} processes are not important in the

method for measuring T_{1n} using a spin echo, to be described later in the chapter, except that if T_{2n} is too short, the apparatus will not be capable of producing a visible echo. (If T_{2n}, for example, is much less than the minimum time t between the two pulses, the echo amplitude will be zero at time 2t.) However, if an echo is visible, the size of the echo will be proportional to the initial magnetization in the z-direction. This forms the basis for the three pulse method for measuring T_{1n}.

Two Pulse Method

Starting with an equilibrium situation, application of a 90° pulse (P1) leads to a free induction decay tail of magnitude $A = A_\infty$. If a second 90° pulse (P2) is applied at a time t later, the amplitude of the FID will depend on the size of the z-component of the magnetization which existed at time t. Repeating the above experiment for various t's, ranging from $t << T_{1n}$ to $t >> T_{1n}$, will result in FID amplitudes from 0 to A_∞. Since A is proportional to M (see Appendix A), A(t) has the same form as Eq. (2.1)

$$A(t) = A_\infty[1-\exp(-t/T_{1n})] \qquad (2.2)$$

From (2.2)

$$\exp(-t/T_{1n}) = 1 - \frac{A}{A_\infty} \qquad (2.3)$$

and

$$\ln(1 - \frac{A}{A_\infty}) = \frac{-t}{T_{1n}} \qquad (2.4)$$

Therefore a plot of $\ln(1 - \frac{A}{A_\infty})$ versus t should yield a straight line of slope $-1/T_{1n}$ passing through ln 1. A sample graph is shown in Fig. 2.2.

The second pulse of the sequence need not be a 90° pulse, since a θ° pulse will still produce some transverse magnetization. The amplitude of the FID will be smaller by a factor of sin θ. It is imperative, however, that P1 be a 90° pulse. Otherwise there would always be a z-component of nuclear magnetization and the interpretation of the FID following the second pulse would be more complicated.

P1 is called a saturating pulse because it reduces the z-component of the nuclear magnetization to zero. If the resonance line width is large, it may be necessary to replace P1 by a string of pulses, called an rf comb.[17] Energy from the pulses is fed into the resonance line at one frequency and diffuses to the rest of the line through cross-relaxation processes. The duration of the comb should be long compared to the cross relaxation time[18] so that the whole line is saturated, otherwise the apparent return to equilibrium will be characteristic of cross-relaxation rather than spin-lattice relaxation processes.

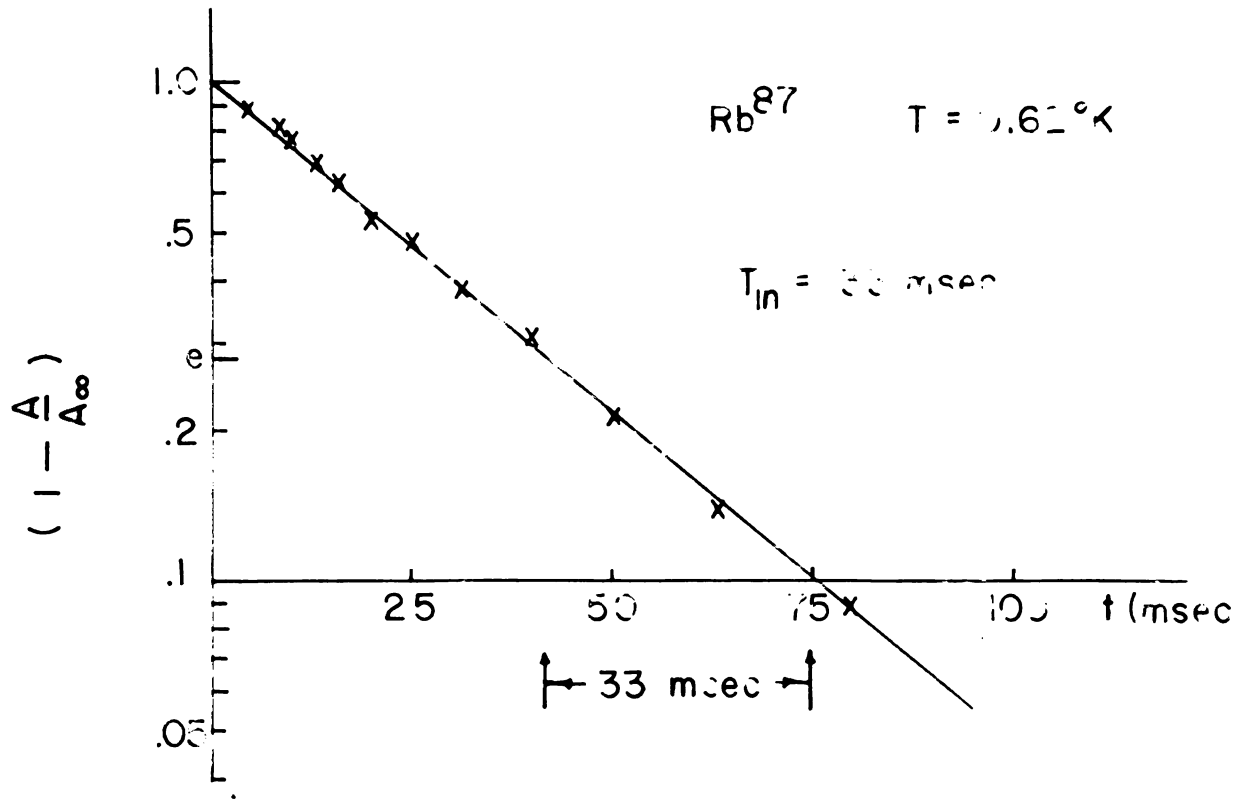

Fig. 2.2. Sample graph for determining T_{1n}.

Three Pulse Method

The three pulse sequence consists of a 90° pulse, P1, followed after time t by an echo forming pair of pulses, (P2) and (P3) respectively. As mentioned above, the size of the echo is proportional to the z-component of nuclear magnetization immediately preceding pulse P2. Therefore if the separation between P1 and P2 is varied from times $t << T_{1n}$ to times $t >> T_{1n}$, the separation between P2 and P3 being kept constant, the amplitude of the echo will change from A = 0 to $A = A_\infty$, where A_∞ is the echo amplitude with pulse P1 turned off. The equation for A as a function of time is the same as that for the two pulse sequence, since in each case A is directly proportional to the z-component of the magnetization existing just before P2. Care must be taken that the sizes and shapes of pulses P2 and P3 do not change when P1 is turned on and off. If they do change, it is a sign that the equipment is incapable of supplying the necessary power. It should be noted that P2 and P3 need not be 90° and 180° pulses respectively in order to form an echo. The 90°-180° case is easy to visualize and was used as an example only. The same technique can be used when P2 and P3 have angles θ_2 and θ_3, as long as a measurable echo is formed. In order that the echo amplitude be as large as possible, the time between P2 and P3 should be much less than T_{1n} and T_{2n}.

The experimental procedure for measuring T_{1n} using the two and three pulses will be given in Chapter III after the apparatus has been discussed.

III. EXPERIMENTAL APPARATUS AND PROCEDURE

In order to measure the nuclear spin-lattice relaxation times of nuclei in antiferromagnetic crystals in the temperature range from 4.2°K to 0.45°K the experimental apparatus must (1) supply sequences of high voltage rf pulses of variable frequency and length to the sample at liquid Helium temperature, (2) pick up, amplify, and display the rf signals induced in the sample by these pulses, (3) be able to maintain a constant temperature during measurements, and (4) allow for measurement of the temperature from 4.2°K to 0.45°K to an accuracy of ±0.005°K. The equipment used falls into two categories, low temperature apparatus and electronic apparatus.

Low Temperature Apparatus

Two systems, a He^3 system and a He^4 system, were used to cover the temperature range from 0.45°K to 4.2°K.

Helium^3 System. Figure 3.1 shows the glass He^3 dewar[19] immersed in liquid He^4. The sample was dropped into position through the He^3 pumping line, oriented by tapping the tip, and held in place by a few drops of Dow Corning 704 fluid which freezes on cooling. Temperatures as low as 0.45°K could be reached by pumping on the

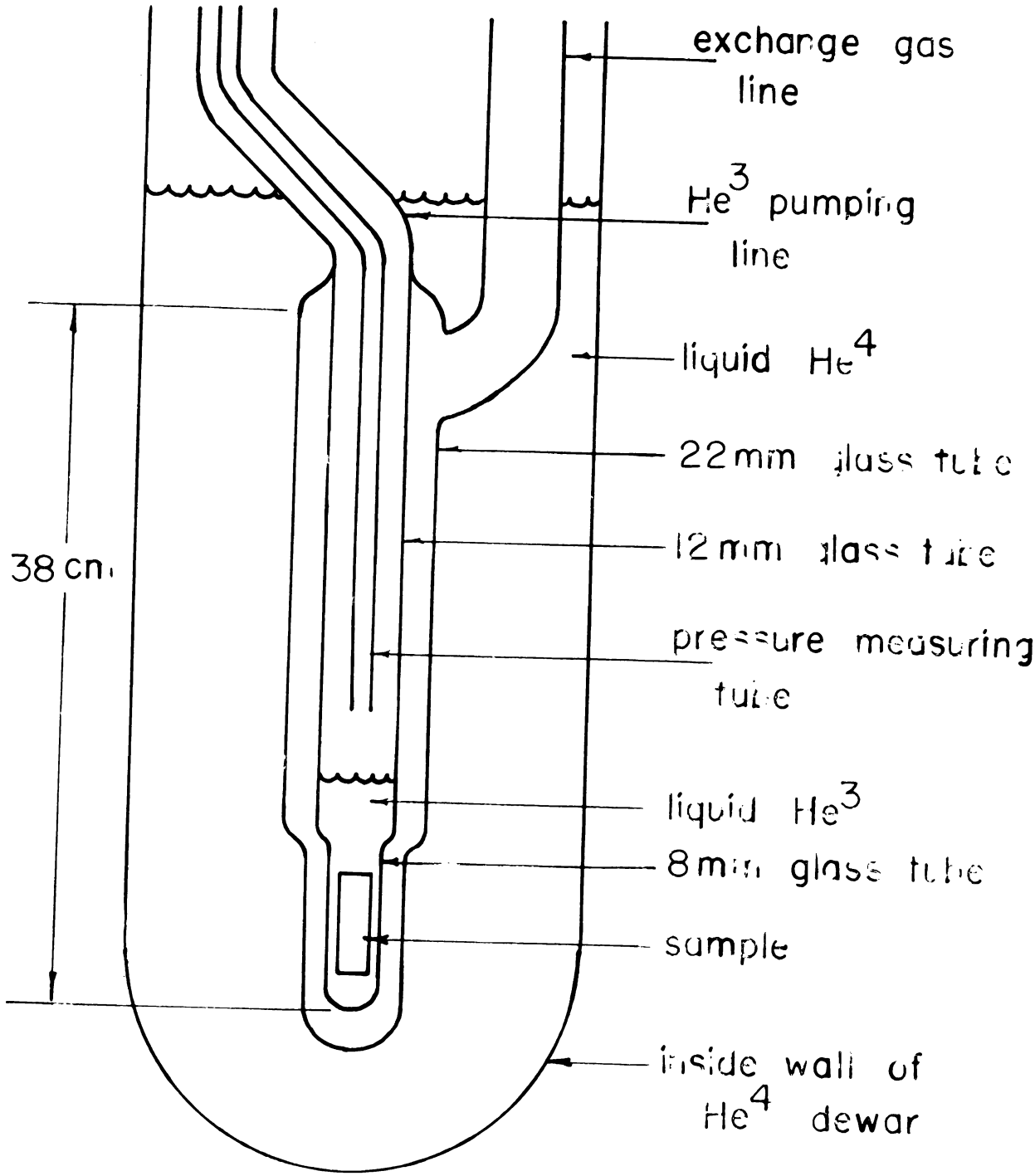

Fig. 3.1. Glass He^3 dewar.

He^3 bath. The temperature was determined by measuring the vapor pressure of the He^3 bath using an NRC Alphatron pressure gauge connected to a 1/8" teflon tube positioned just above the surface of the liquid He^3. A calibration of Alphatron pressure versus temperature was made by measuring the susceptibility of ferric ammonium alum as a function of Alphatron pressure. Ferric ammonium alum obeys the Curie law in the He^3 temperature range. The temperature was determined from the value of the susceptibility at the given pressure. The susceptibility coils[20] shown in Fig. 3.2 were used with the same He^3 dewar in which the T_{1n} measurements were made.

The receiver coil was wrapped around the tip of the He^3 dewar. This meant that the filling factor (see Appendix A) for the coil was much less than one. Since the use of the He^3 dewar was necessary only below 1.17°K (the lower limit of the He^4 system), measurements above this temperature were made in a He^4 system where the receiver coil could be wrapped directly on the sample.

Helium^4 System. The He^4 dewar is shown in Fig. 3.3. The means for transmitting the rf pulses to the sample and receiving the induced signal have been omitted and are shown later. By controlling the pumping rate on the He^4, temperatures from 4.2°K to 1.17°K could be reached and held to an accuracy better than ±0.005°K.

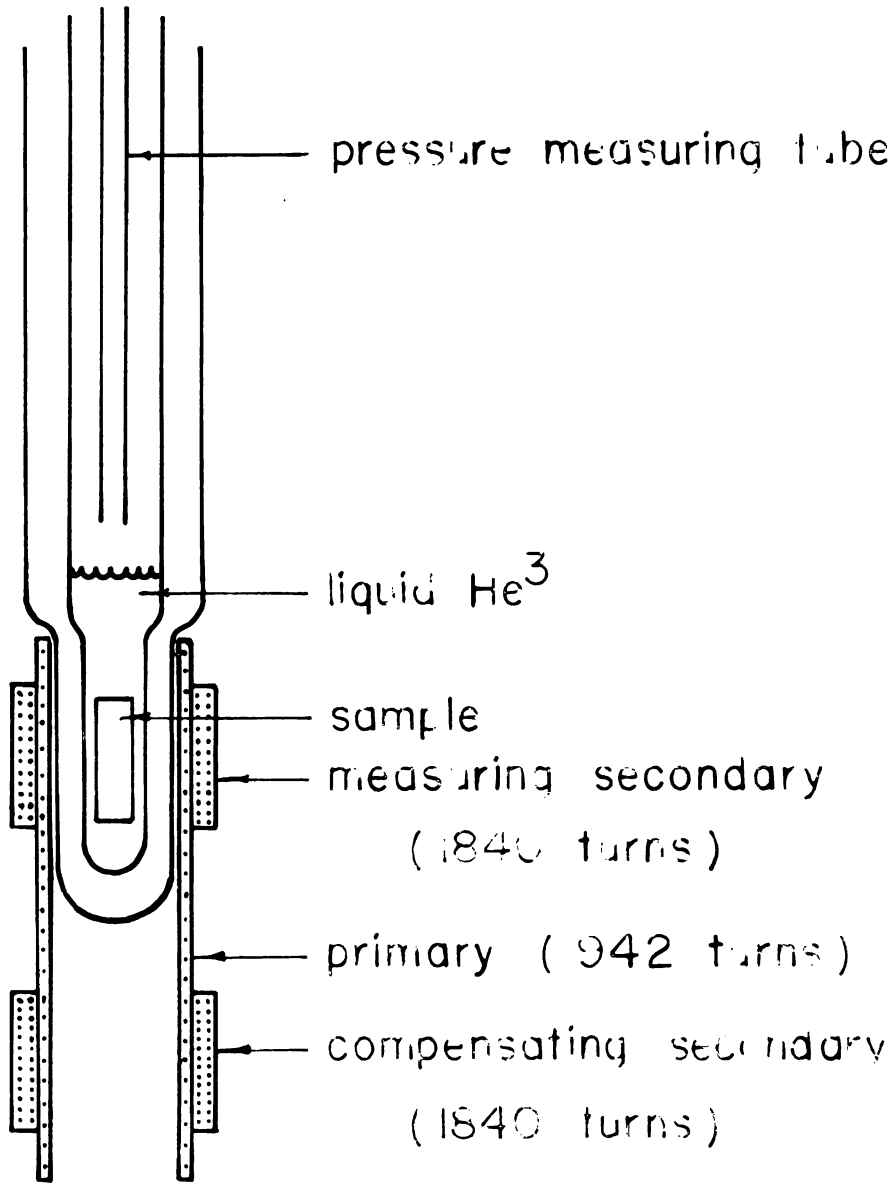

Fig. 3.2. Susceptibility coils.

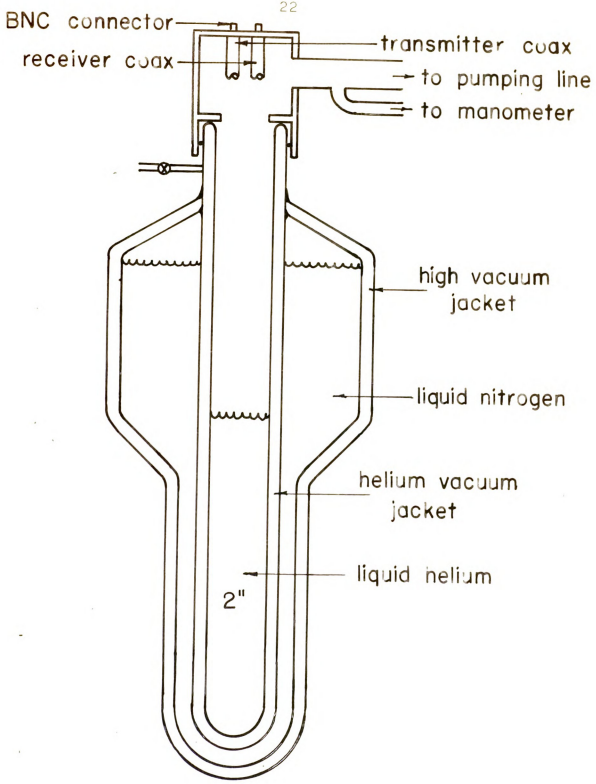

Fig. 3.3. He^4 dewar.

Above about 2.2°K, a mercury manometer was used to measure the vapor pressure of the He^4. Conversion from pressure to temperature was made using the National Bureau of Standards' "1958 He^4 Scale of Temperatures." Below 2.3°K a manometer using oil of known density was used. The ratio of the density of the oil to the density of mercury when multiplied by the height of the oil column gave the pressure in mm of Hg, which was then converted to temperature as above.

Electronic Apparatus

A block diagram of the electronic apparatus is shown in Fig. 3.4. The triggering apparatus provides trigger pulses for the oscilloscope, the amplifier gate circuit and the Arenberg rf oscillator. Rf pulses from the Arenberg are tuned and shaped and fed to the transmitter coil. The small rf voltage induced in the sample by these pulses is picked up by the receiver coil amplified by the rf amplifier, and displayed on the oscilloscope. All connections were made with RG59 and RG62 coaxial cable with BNC connectors. Where low capacitance was a necessity, RG62 cable with a capacitance of 13pf/ft was used.

Triggering Apparatus. Figure 3.5 shows the equipment that generates the trigger pulses for the rf oscillator, the oscilloscope and the rf amplifier gate. The initial trigger pulse is provided by the circuit[21] at the top

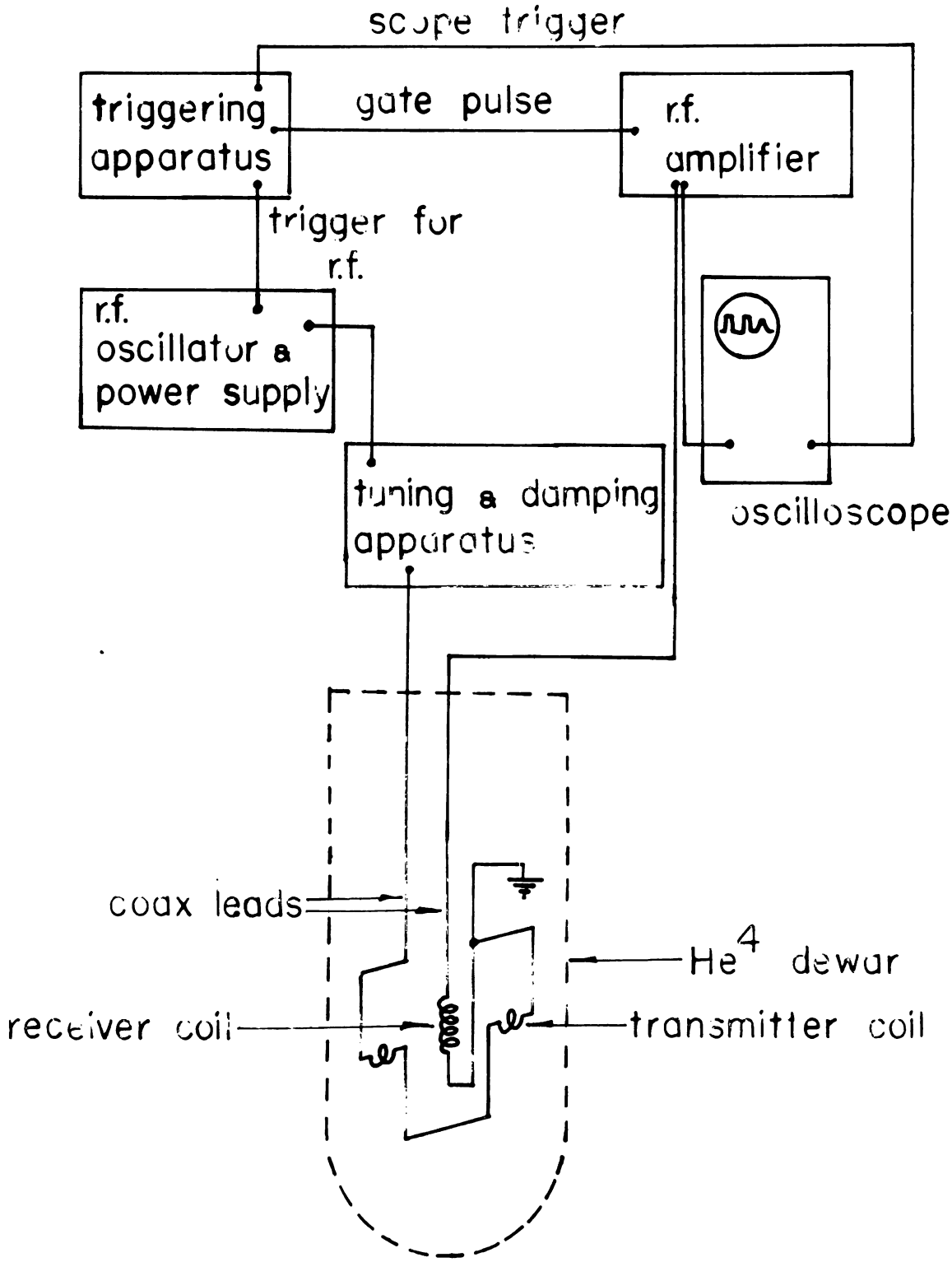

Fig. 3.4. Block diagram of electronic apparatus.

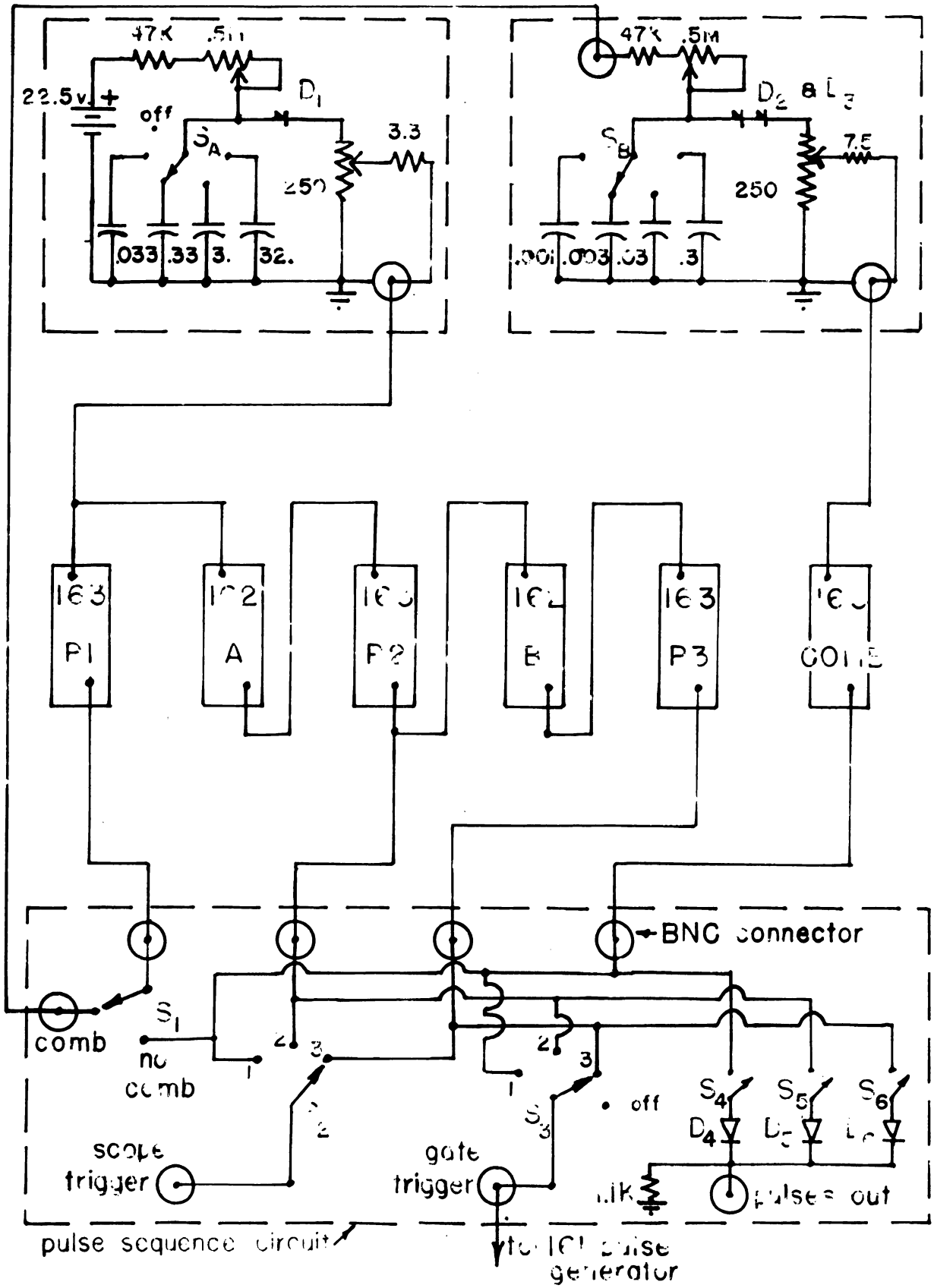

Fig. 3.5. Triggering Apparatus.

left in Fig. 3.5, which uses a 4 layer diode (⊣⊢) (Motorola 463054). This pulse triggers a series of Tektronics 163 pulse generators and Tektronics 162 waveform generators which feed into the pulse sequence circuit shown at the bottom of Fig. 3.5. This circuit permits the sequences shown in Fig. 3.6 to be used. Switch S_1 selects the saturation technique; either an rf "comb" of saturating pulses or a single saturation pulse may be used. Switch S_2 selects the pulse to trigger the oscilloscope and S_3 selects the pulse with which to gate the rf amplifier. Switches S_4, S_5, and S_6 allow any pulse to be turned on or off independently. The diodes in the pulse sequence circuit prevent the pulses from seeing the output impedances of the other pulse generators.

Rf Oscillator. An Arenberg Ultrasonics Laboratory pulsed rf oscillator Model PG-650 was modified to allow external triggering by two or more pulses of varying lengths. High voltage was supplied by a 2500 volt external power supply shown in Fig. 3.7. An rf pulse output power up to 1kW over a frequency range from 3 to 20 MHz was attainable, giving circularly polarized rf magnetic fields (H_1) on the order of 5 gauss. The Arenberg was designed to give a rectangular pulse (i.e., a pulse with no tail) when terminated by a 93Ω termination.

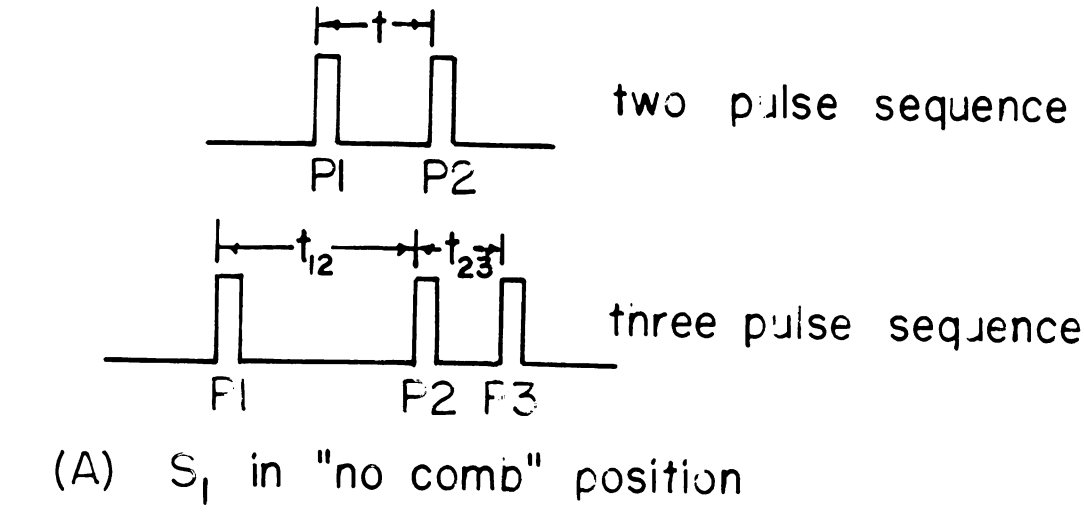

(A) S_1 in "comb" position

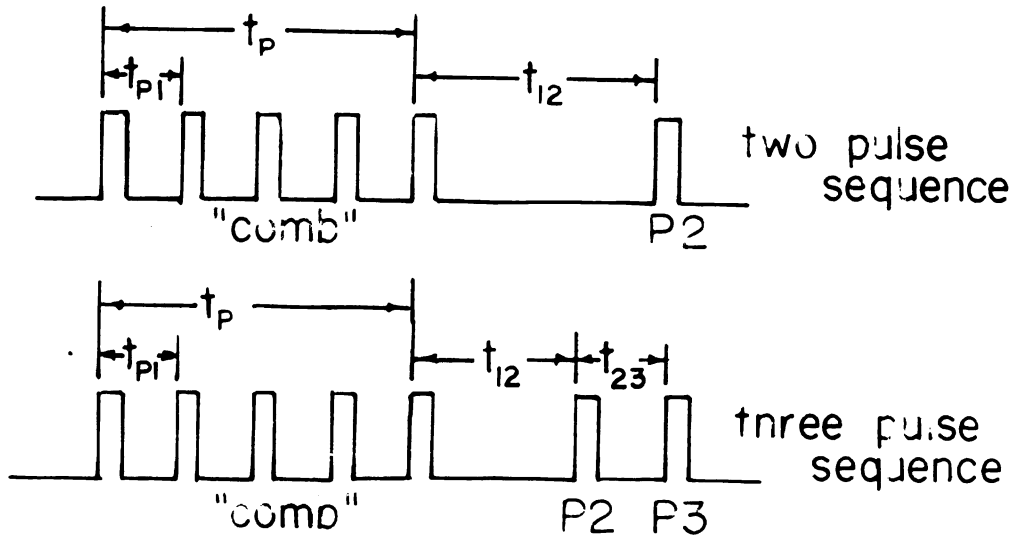

(B) S_1 in "comb" position

Fig. 3.6. Pulse sequences used in measuring T_{1n}.

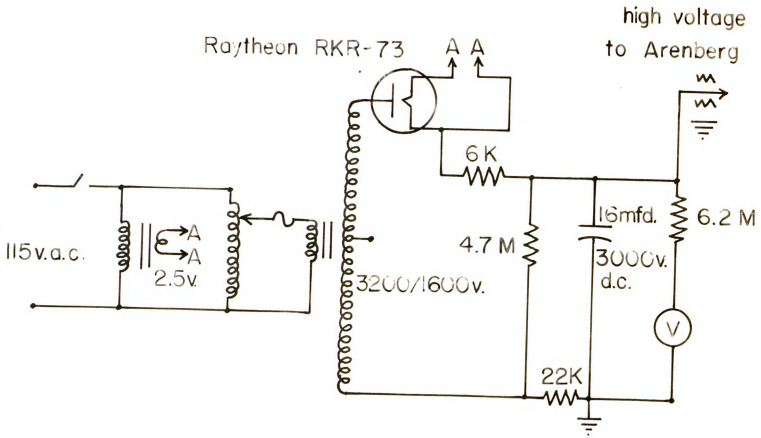

Fig. 3.7. External power supply for rf oscillator.

Tuning and Damping Circuit. A shielded variable air capacitor (15-180 pf) connected in series with the line was used to tune the circuit to series resonance so that the voltage across the transmitter coil was a maximum. Figure 3.8 shows the tuning capacitor and the damper circuit which damps out the ringing induced at the trailing edge of the rf pulse by the series resonant condition. The damper, based on a circuit by Skopas,[22] is essentially two diodes back to back, biased in such a way that the circuit offers low resistance to low voltages and high resistance to high voltages. Thus the Q of the circuit is low during the tail of the pulse and it quickly damps out. Typical pulse shapes are shown in Fig. 3.9.

Transmitter and Receiver Coils. Rf power reached the transmitter coil through a coaxial line (see Fig. 3.10) made from a German silver tube with a number 30 copper wire as the center conductor, the latter insulated with ten gauge teflon insulation. The wire was then threaded through styrofoam cylinders which acted as insulating spacers. The same type of coaxial line was used to carry the rf signal from the receiver coil to the top of the dewar. The capacitance of the lines was kept as small as possible by using the largest size tubing consistent with the space available and the method of supporting the teflon coil from. Table 3-1 shows the size, length and approximate capacitance of each coaxial

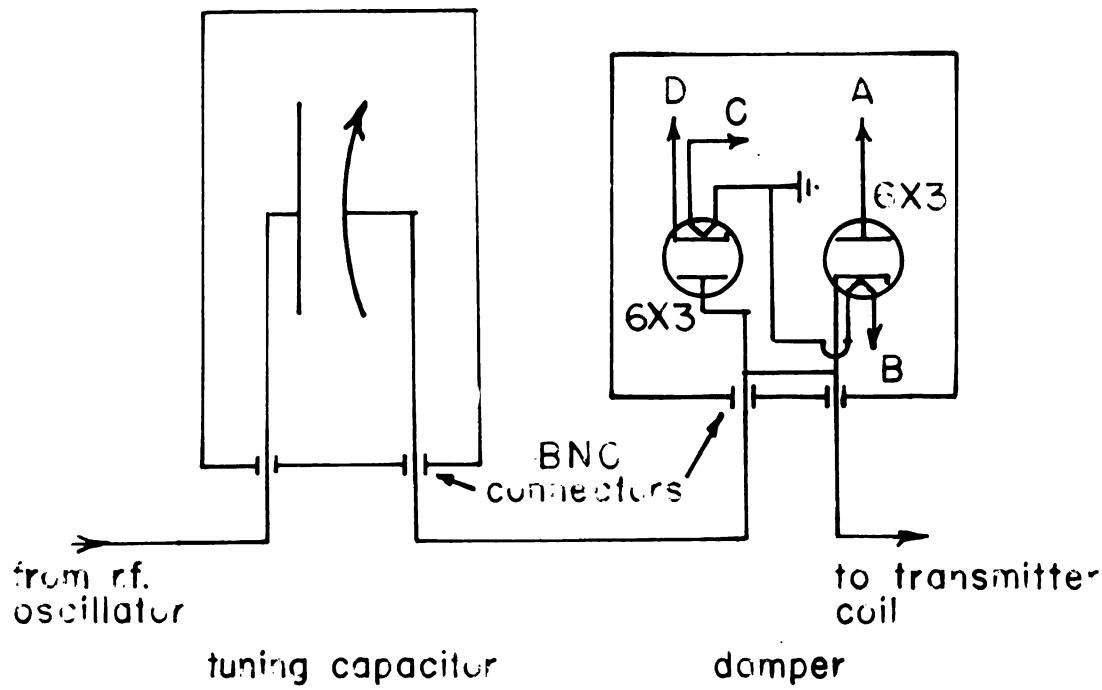

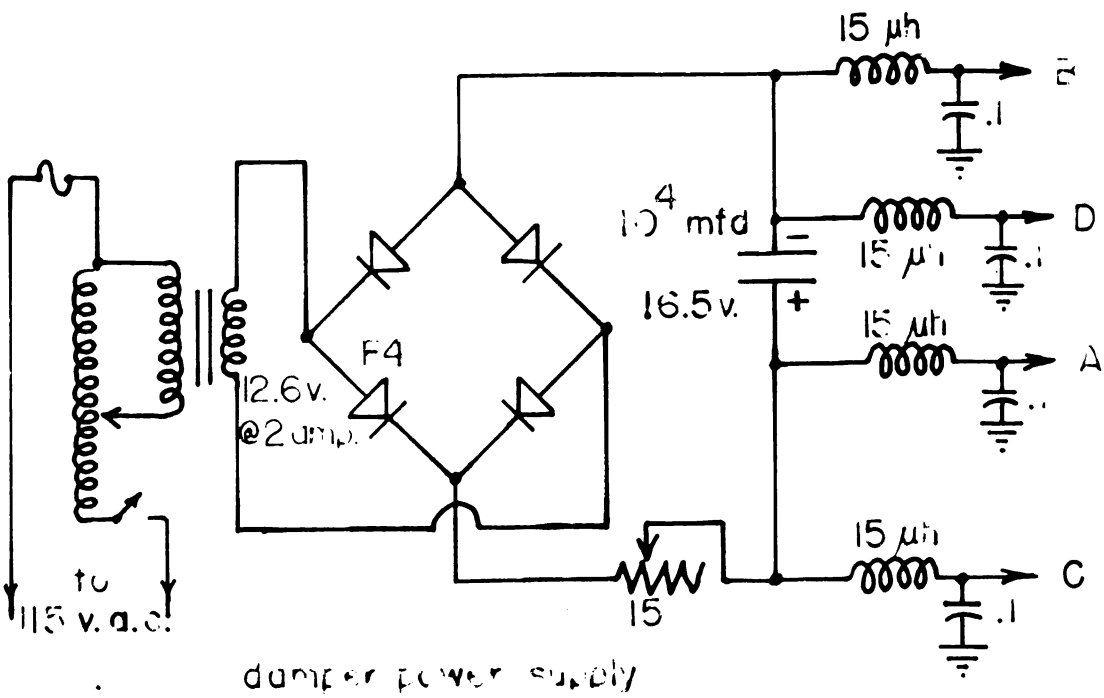

Fig. 3.8. Tuning and damping circuits.

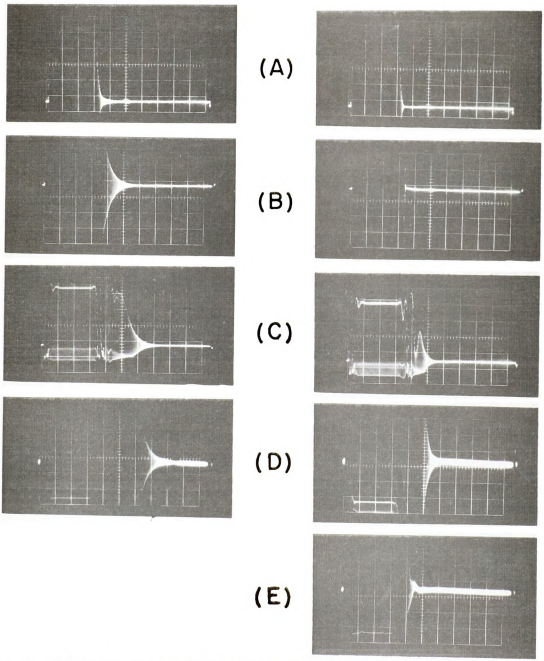

Fig. 3.9 Typical transmitter and receiver outputs for undamped (left) and damped (right) transmitter pulse. Graticle is 6x10cm. x-scale is 5 sec/cm.
(a) and (b) transmitter pulse with y = 100v/cm and 5v/cm
(C) and (D) receiver output with y = 2v/cm and 0.2v/cm
(E) gated receiver output with y = 0.2v/cm

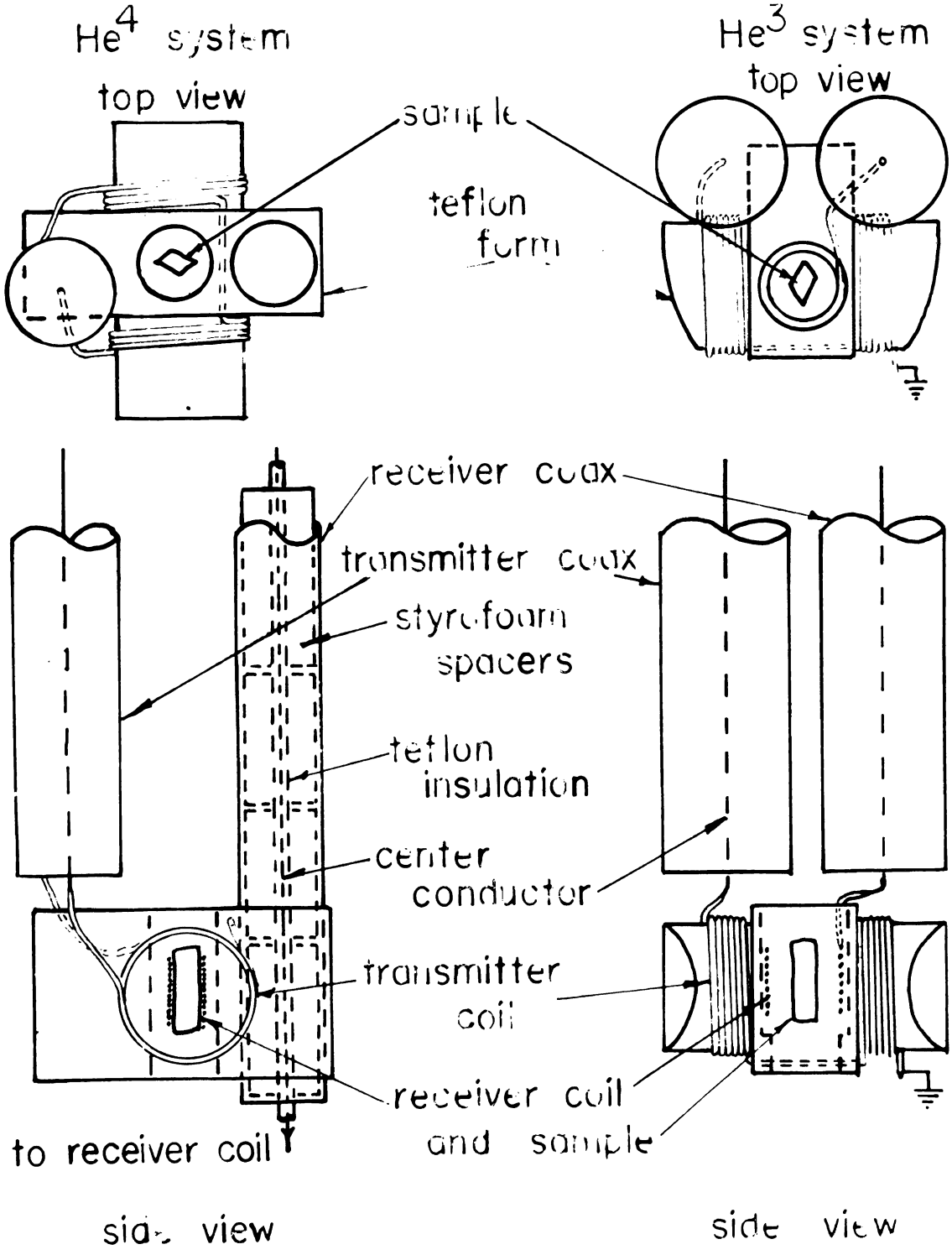

Fig. 3.10. Transmitter and receiver coaxial lines and coils. All coaxial lines have the same construction as that shown for the receiver line in the He^4 system.

Table 3-1

System	Transmitter Coax			Receiver Coax		
	Length (inches)	Diam. (inches)	Cap. (pf)	Length (inches)	Diam. (inches)	Cap. (pf)
He^3	45	3/4	30	45	3/4	30
He^4	37	5/8	30	38½	1/2	35

line in the He^3 and He^4 systems.

The coil form for the transmitter coil was made from teflon. For maximum signal and minimum receiver dead time the coils should be oriented so that (1) the transmitter coil is perpendicular to the internal field $\underline{H}$ at the nucleus under study (so that $\underline{M} \times \underline{H}_1$ is a maximum), (2) the receiver coil is perpendicular to $\underline{H}$ (to get the maximum possible FID after a 90° pulse), and (3) the transmitter and receiver coils are orthogonal (to minimize pickup in the receiver, due to the transmitter pulse). Use of the teflon coil form (Fig 3.10) insured that requirement (3) was reasonably well satisfied. Proper orientation of the crystal, knowing the internal field directions for the different nuclei studied, allowed requirements (1) and (2) to be satisfied to within ±10°.

In the teflon form for the He^3 system, the hole in the center for the sample and receiver coil was made so as to slide easily over the receiver coil and make a firm fit on the tip of the He^3 dewar. For the He^4 system, the sample, with the receiver coil wrapped directly around it, was held in place in the hole in the teflon by two styrofoam wedges, and the teflon form made a firm fit on the receiver coaxial lead.

The number of turns on the transmitter coil for a given frequency range was determined by trial and error,

maximizing the rf pulse voltage in the desired frequency range. Similarly the number of turns on the receiver coil was maximized subject to the condition that the tank circuit of the rf amplifier be tunable over the desired frequency range. Table 3-2 gives the number of turns on receiver and transmitter coils for the different frequencies and systems used.

The teflon form for the Helium^4 system was surrounded by a thin walled brass can which was soldered to the coax leads by means of several criss-crossed wires. This can, not shown in Fig. 3.10, cut down considerably on 60 cycle pickup. The can was open at the top and had holes bored in the bottom so that Helium could flow freely around the sample.

The Rf Amplifier. The induced rf signal was amplified by the circuit shown in Fig. 3.11. The amplification was linear in the range used (output signals up to one volt) and the signal was observed undetected so that A, the amplitude of the signal on the scope, was proportional to A', the amplitude of the induced signal before amplification (see Appendix A). The receiver coil is connected in parallel with tuning capacitor C_T, forming the tank circuit for the amplifier, which can be tuned to the desired frequency. Modifications necessary for good high frequency response (15 to 20 MHz) are indicated in the figure. Because the transmitter

Table 3-2

Frequency Range MHz	Arenberg Oscillator Tank Coil	He^3 System				He^4 System			
		Transmitter Coil		Receiver Coil		Transmitter Coil		Receiver Coil	
		turns/side	diam. (inches)	turns	wire size	turns/side	diam. (inches)	turns	wire size
3-4.5	120JCL	13	3/4	28	#26	12	1	40	#30
6-10	80JCL & 40JCL	4	3/4	16	#26	4	3/4	23	#30
17-19.5	15JCL	2½	3/8	5	#26	--	--	--	--

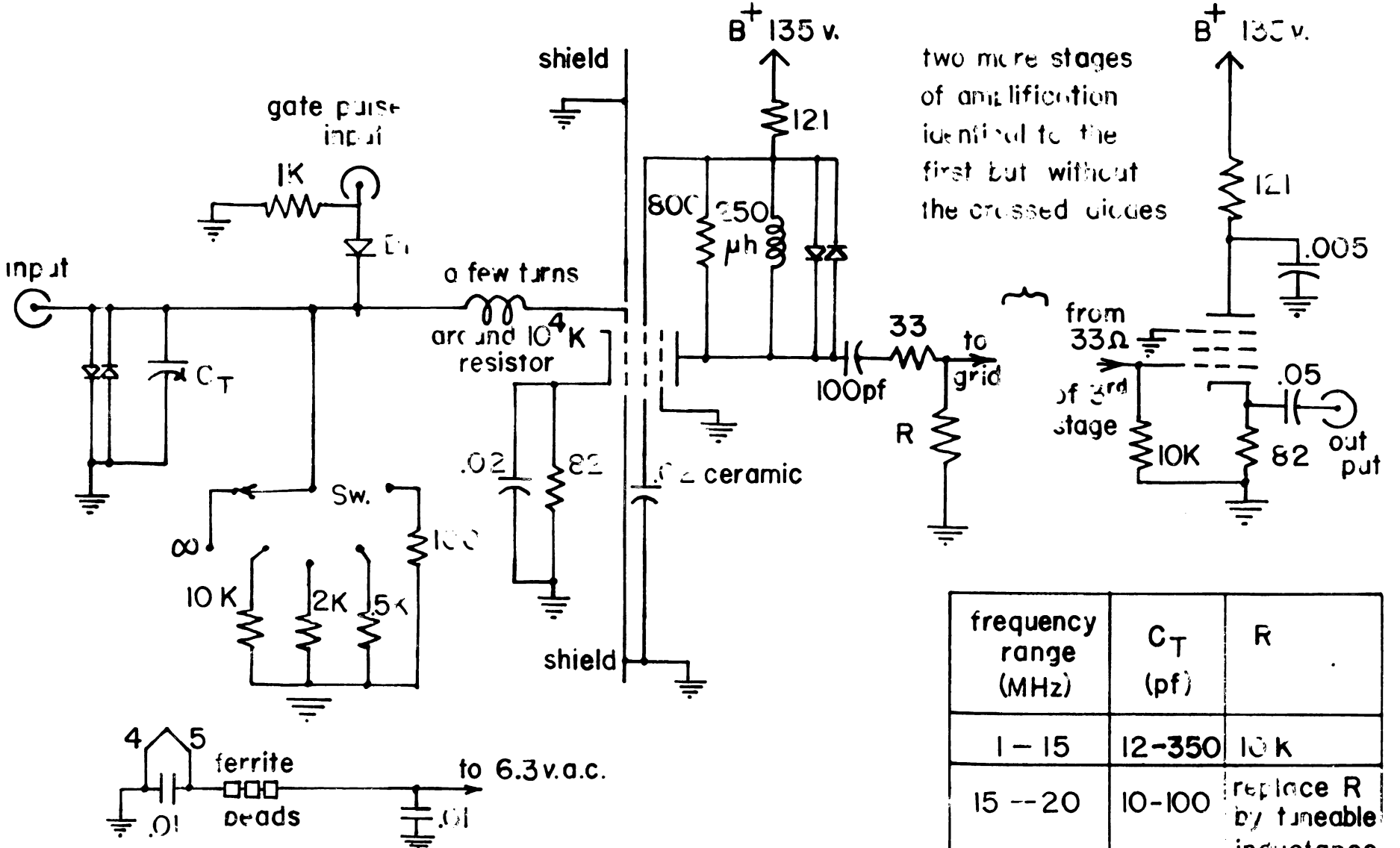

frequency range (MHz)	C_T (pf)	R
1 – 15	12-350	10 k
15 – 20	10-100	replace R by tuneable inductance 1-3 μh

Fig. 3.13. Transmitter.

and receiver coils were not exactly orthogonal, pickup due to the transmitter pulse induced high Q ringing in the tank circuit, saturating the amplifier for as long as 100 microseconds. Crossed diodes at the inputs to the first and second stages were used to cut down on this receiver dead time. It was further cut to less than 15 microseconds and in some cases to about 7 microseconds by gating diode D1, which introduced a low resistance in parallel with the tank circuit. This lowered the Q and damped out the oscillations. The gate pulse was derived from a Tektronics 161 pulse generator and could be triggered to gate the receiver during and after any one of the pulses. It was important that the transmitter pulse have a sharp cut-off to prevent the receiver coil from picking up the ringing tail of the transmitted pulse. To prevent ringing caused by the sharp trailing edge of the gate pulse, a simple shaping circuit, shown in Fig. 3.12, was used, which put a smooth tail on the gate pulse leaving the Tektronics 161. Typical receiver output under various conditions is shown in Fig. 3.9.

Oscilloscope. A Tektronics type 531 oscilloscope with a high gain Tektronics Type H plug-in preamplifier, was used for most of the measurements. In general no scale with sensitivity greater than 0.1 volt/cm was used.

Procedure for Taking Data

The discussion in Chapter II alluded to two different pulse sequences used in measuring T_{1n}. The two

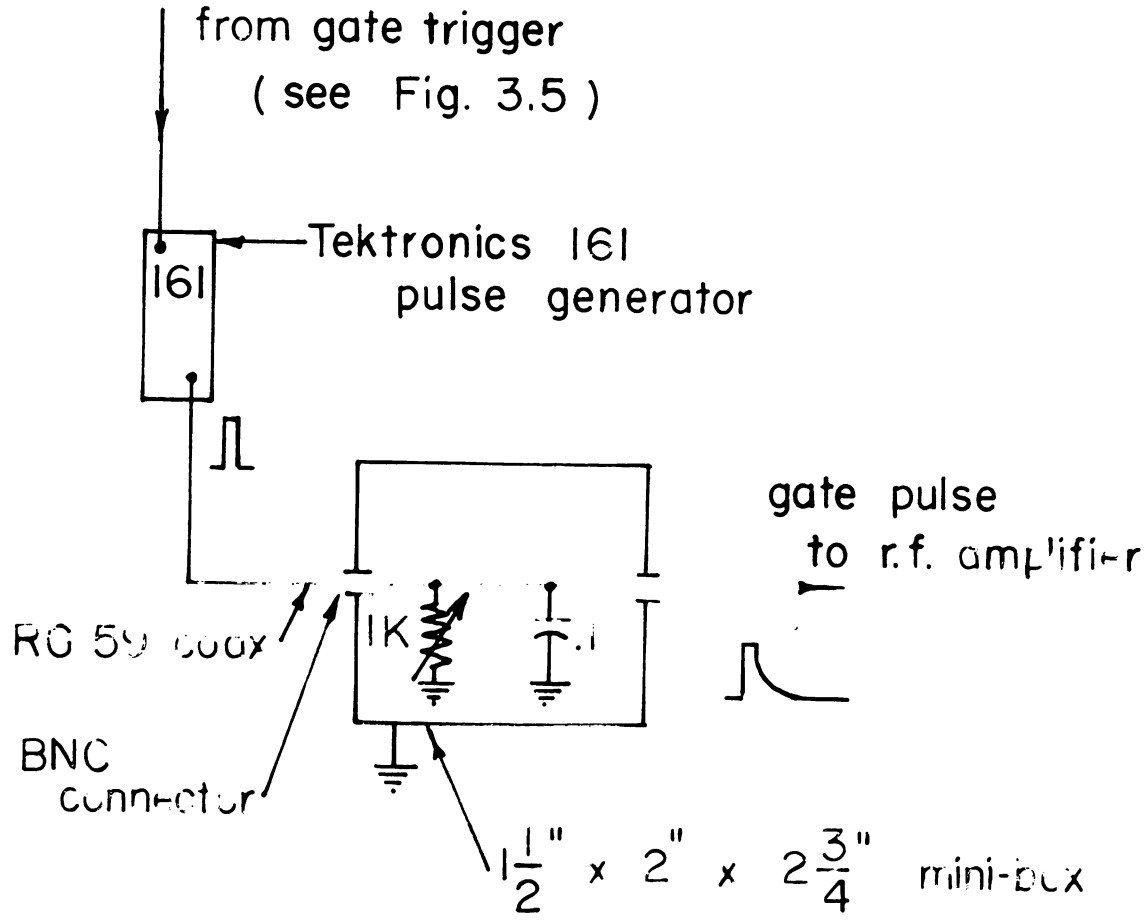

Fig. 3.12. Gate pulse shaping circuit.

pulse method was used when no useable echo signal was obtainable. This was the case for Cl^{35} and proton resonance lines. When a good echo was observed (Rb^{85} and Rb^{87} resonance lines) the three pulse method was used. The procedure followed when taking data is outlined below for both the two pulse and the three pulse methods.

Two Pulse Method.

(1) Come to equilibrium at some temperature T.

(2) With P1 off, tune the transmitter and receiver until the maximum free induction signal is obtained after P2.

(3) Adjust the repetition rate so that the system is in equilibrium before each two pulse sequence.

(4) Turn on P1 so that t_i, the initial time between the two pulses, is short compared to the expected T_{1n}.

(5) With the scope triggered by P2, adjust P1 to a 90° pulse by making it the minimum length that reduces the FID after P2 to zero. It may be necessary to make fine adjustments on the transmitter frequency to do this.

(6) Turn off P1 and record the FID amplitude ($A = A_\infty$) somewhere on the tail subject to the condition that when P1 is turned on, the FID amplitude at that point on the tail is zero when $t = t_i$.

(7) Now record A as a function of t from $t = t_i$ until

A reaches A_∞, and graph this as described in Chapter II. T_{1n} for the given T can then be found from the slope of this graph, as shown in Fig. 2.2.

Three Pulse Method.

(1) Come to equilibrium at some temperature T.

(2) With P1 off, tune the transmitter and receiver until an echo is observed. Adjust the lengths of P2 and P3 and the time between them to give the best echo possible.

(3) Adjust the repetition rate so that the system is in equilibrium before each three pulse sequence.

(4) Turn on P1 with $t = t_i$, the initial time between P1 and P2, short compared to the predicted T_{1n}.

(5) With the scope triggered by P3, increase the length of P1 from zero to the smallest value that makes the echo amplitude go to zero. This will make P1 a 90° pulse. Fine adjustment of the transmitter frequency is advisable at this point.

(6) Turn off pulse P1 and record the echo amplitude. This value is A_∞.

(7) Now turn on P1 and measure A as a function of the separation between P1 and P2, and graph in the same way as for the two pulse sequence. Again, T_{1n} for the given T can be found from the slope of the graph.

IV. RELAXATION THEORY

The nuclear and electron spin systems in an antiferromagnet are coupled by the hyperfine interaction. The strength of the magnetic field at a particular nucleus depends on the type of hyperfine interaction involved. Three types are generally considered,[23] leading to (1) dipolar fields, (2) transferred hyperfine fields, and (3) direct hyperfine fields. Transferred hyperfine fields arise from overlap of the wavefunctions of electrons of nominally non-magnetic atoms and those of electrons of paramagnetic ions. A spatial redistribution of the spin magnetization then occurs with an associated hyperfine interaction.[24] The direct hyperfine fields, produced by the electron spin and orbital moments, exist at the nuclei of magnetic atoms.

The nuclear energy levels are determined by the average internal magnetic field due to the hyperfine interaction and by the electric quadrupole interaction (which may be important for Cl and Rb nuclei). Transitions between these energy levels are induced by the time varying fluctuations of the internal field, which provide the mechanism for spin-lattice relaxation of the nuclear spin system. The non-static part of the internal field,

taken as a perturbation, is produced by thermal fluctuations in the electron spin system and can thus be described, at sufficiently low temperatures, by non-interacting magnons. In this chapter we introduce expressions for the electron spin operators in terms of magnon creation and annihilation operators and derive the magnon dispersion relation. We then discuss magnon relaxation mechanisms and their dependence on the magnon dispersion relation, introduce the perturbation Hamiltonian and the total static Hamiltonian, and derive an expression for T_{1n} based on the two magnon (Raman) relaxation mechanism.

Magnon Operators

The transformation from electron spin variables S^+, S^- and S^z to magnon variables A^+_{kp} and A_{kp} is discussed in many references.[25,26,27] The following discussion is adapted from Kittel.[27] Consider that N electron spins lie on two interpenetrating sublattices, q and r, such that the N/2 spins on sublattice q are aligned in the + z-direction and the N/2 spins on sublattice r are aligned in the - z-direction. Further, consider the case where the nearest neighbors of a spin on sublattice q are all on sublattice r and vice versa. In the absence of an applied magnetic field, the Hamiltonian for the electron spin system is

$$\mathcal{H}_E = -2J \sum_{i<j} \underline{S}_i \cdot \underline{S}_j - 2\mu_o H_A \sum_j S^z_{qj} + 2\mu_o H_A \sum_j S^z_{rj} \qquad (4.1)$$

where J is the nearest neighbor exchange integral, μ_o is the Bohr magneton and H_A is a fictitious magnetic field which aligns spins on sublattice q in the + z-direction and spins on sublattice r in the - z-direction, thus representing the effect of the crystalline anisotropy.[28]

We now express the electron spin operators $S^+ = S_x + iS_y$ and $S^- = S_x - iS_y$ in terms of spin-deviation creation and annihilation operators using the Holstein-Primakoff transformation.[29]

$$S^+_{qj} = (2S)^{\frac{1}{2}}(1 - a^+_{qj}a_{qj}/2S)^{\frac{1}{2}}a_{qj} \qquad (4.2)$$

$$S^-_{qj} = (2S)^{\frac{1}{2}}a^+_{qj}(1 - a^+_{qj}a_{qj}/2S)^{\frac{1}{2}} \qquad (4.3)$$

$$S^+_{r\ell} = (2S)^{\frac{1}{2}}a^+_{r\ell}(1 - a^+_{r\ell}a_{r\ell}/2S)^{\frac{1}{2}} \qquad (4.4)$$

$$S^-_{r\ell} = (2S)^{\frac{1}{2}}(1 - a^+_{r\ell}a_{r\ell}/2S)^{\frac{1}{2}}a_{r\ell} \qquad (4.5)$$

The operator a^+_{qj} creates one unit of spin deviation on the j^{th} electron on sublattice q, and $a_{r\ell}$ destroys one unit of spin deviation on the ℓ^{th} electron on sublattice r. The spin deviation operators obey boson commutation relations

$$[a_{ij}, a^+_{h\ell}] = \delta_{ih}\delta_{j\ell} \; ; \quad i = q,r; \; h = q,r \qquad (4.6)$$

In (4.4) the operator $a^+_{r\ell}$ has been associated with $S^+_{r\ell}$ because we want both S^+_{qj} and $S^+_{r\ell}$ to result in an increase in the total + z-component of the electron magnetization. Similarly $a_{r\ell}$ has been associated with $S^-_{r\ell}$. Using the identity $S_j \cdot S_j = S(S+1)$ and Eq. (4-6) one can calculate

$$S^z_{qj} = S - a^+_{qj} a_{qj} \tag{4.7}$$

$$S^z_{r\ell} = -S + a^+_{r\ell} a_{r\ell} \tag{4.8}$$

The operator $a^+_{qj} a_{qj}$ operating on an eigenstate of the system gives the number of spin deviations on the j^{th} electron of the q sublattice.[29] It is therefore called the number operator. Thus the expectation value of S^z_{qj} is given by the value of S minus the expectation value of the number of spin deviations on atom j of the q sublattice.

We now transform to spin-wave variables b_{ik}, b^+_{ik}, which destroy and create magnons of wave vector $\underline{k}$ on the i^{th} sublattice, i = q,r. The transformations are

$$b_{qk} = \left(\frac{2}{N}\right)^{\frac{1}{2}} \sum_j e^{+i\underline{k}\cdot\underline{r}_j} a_{qj} \tag{4.9}$$

$$b^+_{qk} = \left(\frac{2}{N}\right)^{\frac{1}{2}} \sum_j e^{-i\underline{k}\cdot\underline{r}_j} a^+_{qj} \tag{4.10}$$

$$b_{rk} = \left(\frac{2}{N}\right)^{\frac{1}{2}} \sum_\ell e^{-i\underline{k}\cdot\underline{r}_\ell} a_{r\ell} \tag{4.11}$$

$$b^+_{rk} = \left(\frac{2}{N}\right)^{\frac{1}{2}} \sum_\ell e^{+i\underline{k}\cdot\underline{r}_\ell} a^+_{r\ell} \tag{4.12}$$

Thus, qualitatively the magnon creation operator creates a spin deviation on each site of one sublattice and imposes a definite phase relationship on the spin deviations through the sinusoidal term.

If we assume that the number of spin deviations is small, i.e., that $\langle a^{+}_{qj} a_{qj} \rangle / S \ll 1$ we can expand the square root in each of Eqs. (4.2) through (4.5). This constitutes the spin-wave approximation. This gives for (4.2),

$$S^{+}_{qj} = (2S)^{\frac{1}{2}} \left(a_{qj} - \frac{a^{+}_{qj} a_{qj} a_{qj}}{4S} + \ldots \right) \tag{4.13}$$

Using the inverse of the transformations (4.9) and (4.10) we have, neglecting third and higher order magnon terms

$$S^{+}_{qj} = \left(\frac{4S}{N} \right)^{\frac{1}{2}} \sum_{k} e^{-i\underline{k} \cdot \underline{r}_j} b_{qk} + \ldots \tag{4.14}$$

Similarly

$$S^{-}_{qj} = \left(\frac{4S}{N} \right)^{\frac{1}{2}} \sum_{k} e^{-i\underline{k} \cdot \underline{r}_j} b^{+}_{qk} + \ldots \tag{4.15}$$

$$S^{+}_{r\ell} = \left(\frac{4S}{N} \right)^{\frac{1}{2}} \sum_{k} e^{-i\underline{k} \cdot \underline{r}_\ell} b^{+}_{rk} + \ldots \tag{4.16}$$

$$S^{-}_{r\ell} = \left(\frac{4S}{N} \right)^{\frac{1}{2}} \sum_{k} e^{+i\underline{k} \cdot \underline{r}_\ell} b_{rk} + \ldots \tag{4.17}$$

From (4.7) through (4.12) we have

$$S^{z}_{qj} = S - \left(\frac{2}{N} \right) \sum_{kk'} e^{i(\underline{k}-\underline{k}') \cdot \underline{r}_j} b^{+}_{qk} b_{qk'} + \ldots \tag{4.18}$$

$$S^{z}_{r\ell} = -S + \left(\frac{2}{N} \right) \sum_{kk'} e^{-i(\underline{k}-\underline{k}') \cdot \underline{r}_\ell} b^{+}_{rk} b_{rk'} + \ldots \tag{4.19}$$

Notice that S^+ and S^- involve odd numbers of magnon operators while S^z involves an even number.

If we now express $\mathcal{H}_E$ from (4.1) in terms of magnon variables, we find that, assuming nearest neighbor coupling only

$$\mathcal{H}_E = \mathcal{H}_o + \mathcal{H}_1' + \text{constant terms} \tag{4.20}$$

where $\mathcal{H}_1'$ represents higher order magnon terms (three or more) and

$$\mathcal{H}_o = -2JzS\sum_k [\gamma_k(b_{qk}^+ b_{rk}^+ + b_{qk}b_{rk}) + (b_{qk}^+ b_{qk} + b_{rk}^+ b_{rk})]$$

$$+ 2\mu_o H_A \sum_k (b_{qk}^+ b_{qk} + b_{rk}^+ b_{rk}) \tag{4.21}$$

$$\gamma_k = \frac{1}{z}\sum_{\underline{\delta}} e^{i\underline{k}\cdot\underline{\delta}} = \gamma_{-k} \tag{4.22}$$

The vector $\underline{\delta}$ connects a given spin with its z nearest neighbors and we have assumed that the crystal has a center of symmetry. In arriving at (4.20) identities of the following form have been used.[30]

$$\sum_j e^{i(\underline{k}-\underline{k}')\cdot r_j} = \frac{N}{2}\delta_{kk'} \tag{4.23}$$

$$\sum_{jkk'} e^{i(\underline{k}-\underline{k}')\cdot r_j} b_{qk}^+ b_{qk'} = \frac{N}{2}\sum_k b_{qk}^+ b_{qk} \tag{4.24}$$

(4.23) can be proved by writing out the sum explicitly and grouping the terms in sums of geometric progressions. (4.24) follows directly. Because of terms like

$b^+_{qk}b^+_{rk}$, Eq. (4.20) is not diagonal as it stands. The transformation which diagonalizes $\mathcal{H}_o$ is defined by

$$b_{qk} = c_{k1}A_{k1} + c_{k2}A^+_{k2} \tag{4.25}$$

$$b_{rk} = c_{k1}A_{k2} + c_{k2}A^+_{k1} \tag{4.26}$$

$$b^+_{qk} = c_{k1}A^+_{k1} + c_{k2}A_{k2} \tag{4.27}$$

$$b^+_{rk} = c_{k1}A^+_{k2} + c_{k2}A_{k1} \tag{4.28}$$

where c_{k1}, c_{k2} are real and must satisfy $c_{k1}^2 - c_{k2}^2 = 1$. The latter equation insures that $[A_{kp}, A^+_{\ell p'}] = \delta_{k\ell}\delta_{pp'}$. This is the boson commutation relation. Substitution of (4.25) through (4.28) in (4.21) shows that the off-diagonal terms cancel if

$$c_{k1} = \frac{\rho_k}{(\rho_k^2 - \gamma_k^2)^{\frac{1}{2}}} \qquad c_{k2} = \frac{-\gamma_k}{(\rho_k^2 - \delta_k^2)^{\frac{1}{2}}} \tag{4.29}$$

$$\rho_k = 1 + \frac{\omega_A}{\omega_e} + \left[\left(1 + \frac{\omega_A}{\omega_e}\right)^2 - \gamma_k^2\right]^{\frac{1}{2}} \tag{4.30}$$

where $\omega_e = 2JzS$ and $\omega_A = 2\mu_o H_A$. Using the boson commutation relations and substituting Eqs. (4.25) through (4.30) in (4.21), we get

$$\mathcal{H}_o = \sum_k \omega_k (A^+_{k1}A_{k1} + A^+_{k2}A_{k2} + 1) \tag{4.31}$$

with ω_k given by

$$\omega_k = [(\omega_e + \omega_A)^2 - \omega_e{}^2\gamma_k{}^2]^{\frac{1}{2}} \tag{4.32}$$

Eq. (4.32) is the dispersion relation for antiferromagnetic magnons which is discussed in the next section.

In the diagonalized representation, for each magnon of wavevector $\underline{k}$, there are two degenerate modes, p, where p = 1,2. The operator A^+_{kp} creates a magnon of wavevector $\underline{k}$ and polarization p; A_{kp} annihilates the same magnon. Notice that it is not as simple to "picture" these magnons as it was when a given magnon was confined to one sublattice. The operator $A^+_{kp}A_{kp}$ when operating on an eigenstate of the electron spin system gives the number of magnons of wavevector $\underline{k}$ and polarization p in that system. This can be derived by considering an eigenstate $|...n_{kp}...)$ in which there are n_{kp} magnons present in the mode $\underline{k}_p$, where $\underline{k}$ runs over the N/2 wavevectors and p = 1,2. From magnon theory[31] we have

$$A^+_{kp}|...n_{kp}...) = (n_{kp} + 1)^{\frac{1}{2}}|...n_{kp} + 1...) \tag{4.33}$$

$$A_{kp}|...n_{kp}...) = (n_{kp})^{\frac{1}{2}}|...n_{kp} - 1...) \tag{4.34}$$

Therefore

$$A^+_{kp}A_{kp}|...n_{kp}...) = (n_{kp})^{\frac{1}{2}}(n_{kp})^{\frac{1}{2}}|...n_{kp}...) \tag{4.35}$$

and

$$A^+_{kp}A_{kp} = n_{kp} \tag{4.36}$$

We can then write $\mathcal{H}_o$ in (4.31) as

$$\mathcal{H}_o = \sum_k \omega_k(n_{k1} + \tfrac{1}{2}) + \sum_k \omega_k(n_{k2} + \tfrac{1}{2}) \tag{4.37}$$

To express the spin operators in terms of the magnon operators in the diagonalized representation we substitute Eqs. (4.24) through (4.27) into (4.14) through (4.19). Neglecting third and higher order terms, we have

$$S^+_{qj} = \left(\frac{4S}{N}\right)^{\frac{1}{2}} \sum_k e^{-i\underline{k}\cdot\underline{r}_j}(c_{k1}A_{k1} + c_{k2}A^+_{k2}) \tag{4.38}$$

$$S^-_{qj} = \left(\frac{4S}{N}\right)^{\frac{1}{2}} \sum_k e^{+i\underline{k}\cdot\underline{r}_j}(c_{k1}A^+_{k1} + c_{k2}A_{k2}) \tag{4.39}$$

$$S^+_{r\ell} = \left(\frac{4S}{N}\right)^{\frac{1}{2}} \sum_k e^{-i\underline{k}\cdot\underline{r}_\ell}(c_{k1}A^+_{k2} + c_{k2}A_{k1}) \tag{4.40}$$

$$S^-_{r\ell} = \left(\frac{4S}{N}\right)^{\frac{1}{2}} \sum_k e^{+i\underline{k}\cdot\underline{r}_\ell}(c_{k1}A_{k2} + c_{k2}A^+_{k1}) \tag{4.41}$$

$$S^z_{qj} = S - \left(\frac{2}{N}\right) \sum_{kk'} e^{i(\underline{k}-\underline{k}')\cdot\underline{r}_j}(c_{k1}A^+_{k1} + c_{k2}A_{k2})$$

$$\times\ (c_{k'1}A_{k'1} + c_{k'2}A^+_{k'2}) \tag{4.42}$$

$$S^z_{r\ell} = -S + \left(\frac{2}{N}\right) \sum_{kk'} e^{-i(\underline{k}-\underline{k}')\cdot\underline{r}_\ell}(c_{k1}A^+_{k2} + c_{k2}A_{k1})$$

$$\times\ (c_{k'1}A_{k'2} + c_{k'2}A^+_{k'1}) \tag{4.43}$$

The Magnon Dispersion Relation

The dispersion relation for antiferromagnetic magnons

was given in Eq. (4.32) and is repeated here for convenience.

$$\omega_k = [(\omega_e + \omega_A)^2 - \omega_e{}^2\gamma_k{}^2]^{\frac{1}{2}} \tag{4.44}$$

It is customary to write this in the small k approximation using $\gamma_k{}^2 = 1 - bk^2$, which is obtained from the definition of γ_k, (4.22), by expanding the exponential to second order in $\underline{k}$, and squaring the result, again keeping only terms to second order in $\underline{k}$. If there is a center of symmetry in the crystal, linear terms in the sum will cancel. Then

$$\omega_k = [\omega_e{}^2 bk^2 + 2\omega_e\omega_A + \omega_A{}^2]^{\frac{1}{2}} \tag{4.45}$$

An important feature of this dispersion relation is that for k = 0, we have

$$\omega_k = [2\omega_E\omega_A + \omega_A{}^2]^{\frac{1}{2}} \tag{4.46}$$

so that there is an energy gap in the magnon spectrum. The effect of the gap is to suppress the excitation of magnons for temperatures T less than T_{AE}, where T_{AE} is defined by

$$k_B T_{AE} = \hbar\omega_{k=0} \tag{4.47}$$

The general shape of the dispersion relation in the first Brillouin zone is shown in Fig. 4.1. The dashed line is the long wavelength (small k) approximation to $\hbar\omega_k$ disregarding Brillouin zone effects and assuming $\omega_A = 0$. Note that the larger T_{AE} is, the flatter will be the dispersion curve.

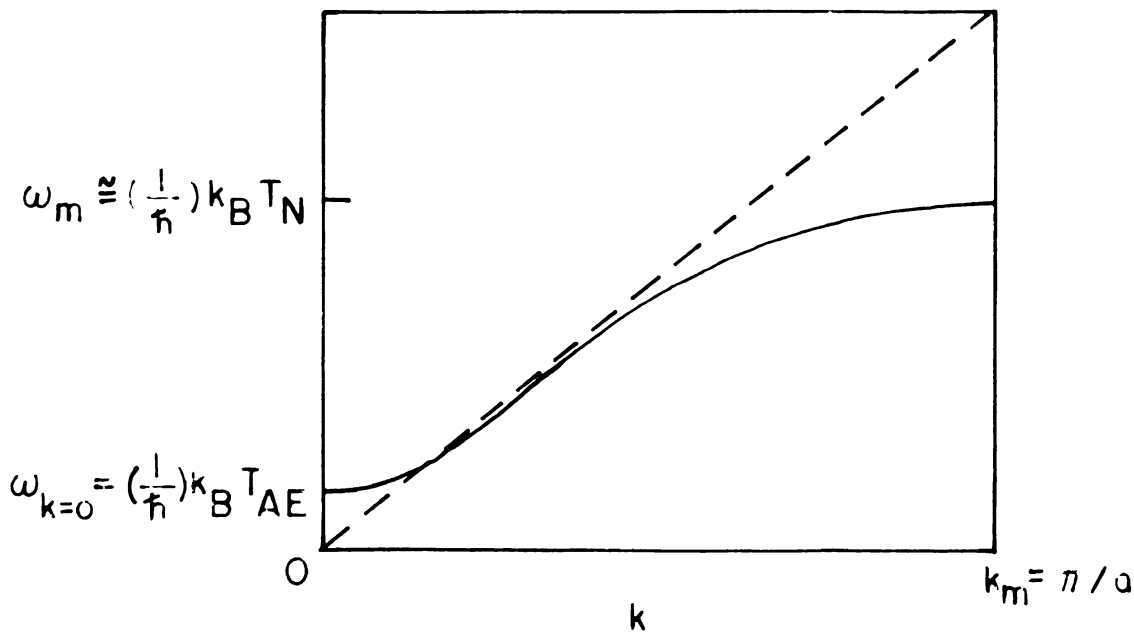

Fig. 4.1. Typical dispersion curve for antiferromagnetic magnons.

Magnon Relaxation

At temperatures low enough that the spin wave approximation is valid, relaxation of a nuclear spin might be expected to occur via one magnon (direct), two magnon (Raman), three magnon, or higher order relaxation mechanisms. In the direct process, the nuclear spin flips and a magnon of wavevector $\underline{k}$ and energy $\hbar\omega_L$, where ω_L is the nuclear resonance frequency, is emitted. Such processes involve a magnon creation operator A_k^+. The two magnon process can be described as magnon scattering; a magnon of wave vector $\underline{k}$ is absorbed, the nuclear spin flips and a magnon of wavevector $\underline{k}'$ is emitted where $E_k = E_{k'} - \hbar\omega_L$. This requires two-magnon terms like $A_k A_{k'}^+$ in the perturbing Hamiltonian. Three magnon processes involve terms like $A_k^+ A_{k'}, A_{k''}$ which represents the absorption of two magnons (wavevector k' and k"), the creation of one magnon (wavevector k) and a simultaneous flip by the nuclear spin. Conservation of energy requires in this case

$$E_{k'} + E_{k''} = E_k - \hbar\omega_L \qquad (4.48)$$

In discussing the importance of these three relaxation mechanisms it is necessary to consider the effect of the antiferromagnetic magnon dispersion relation. First consider the effect of the energy gap on the direct process. A nuclear resonance frequency of 10MHz corresponds to a temperature of about 10^{-3}°K. This is

well below T_A in almost all antiferromagnets so that it is generally impossible to have a direct process and still conserve energy.

Next consider the effect of a large energy gap on the three magnon process. For $T_{AE} \simeq T_N$, the magnon spectrum will be essentially flat and again it will be impossible to conserve energy.[32] For T_{AE} large, we are left with the two magnon process as the dominant relaxation mechanism.

The Perturbation Hamiltonian

Relaxation of the nuclear spin system occurs through hyperfine coupling of the nuclei to the fluctuations in the electron spin system. In this section we discuss the Hamiltonian which will be used as a perturbation in calculating T_{1n}. We will consider only the dipolar contribution to the hyperfine interaction. The formalism for transferred hyperfine interaction is the same; only the coupling terms are different. The Hamiltonian for the hyperfine interaction $\mathcal{H}_1$ is then

$$\mathcal{H}_1 = -\gamma_N \hbar \underline{T} \cdot \underline{I} \tag{4.49}$$

$$\underline{T} = \sum_i d_i [\underline{S}_i - \left(\frac{3}{r_i^2}\right) (\underline{S}_i \cdot \underline{r}_i) \underline{r}_i] \tag{4.50}$$

where $d_i = -\gamma_e \hbar / r_i^3$, r_i is the vector joining the nucleus and the i^{th} spin and the sum runs over all electron spins.

$\underline{T}$ is the operator which represents the magnetic field at the nucleus due to all the electron spins. We have tacitly assumed that the interactions between the nuclei can be neglected, since they are small compared to the hyperfine interaction. Further we assume that the interaction $\mathcal{H}_1$ has little effect on the motion of the atomic spins.

By writing $\underline{S}_i = \langle \underline{S}_i \rangle + \underline{S}_i)$, $\underline{T}$ may be split into a constant part $\underline{U}$ and a fluctuating part $\underline{V}$. The eigenstates $|\chi_n)$ of the nucleus are then determined by $\mathcal{H}_U$, the static part of $\mathcal{H}_1$, given by

$$\mathcal{H}_U = -\gamma_N \hbar \underline{U} \cdot I \tag{4.51}$$

where U is identical to Eq. (4.50) with $\underline{S}_i$ replaced by $\langle \underline{S}_i \rangle$. Transitions between the eigenstates are induced by the fluctuating part of $\mathcal{H}_1$ and it is these transitions that contribute to the relaxation of the nuclear spin system. We can write the fluctuating part of $\mathcal{H}_1$ as

$$\mathcal{H}_V = -\gamma_N \hbar \underline{V} \cdot \underline{I} \tag{4.52}$$

$$\underline{V} = \sum_i d_i [\delta \underline{S}_i - \left(\frac{3}{r_i}\right)^2 (\delta \underline{S}_i \cdot \underline{r}_i) \underline{r}_i] \tag{4.53}$$

where

$$\delta \underline{S}_i = \underline{S}_i - \langle S_i \rangle \tag{4.54}$$

The Total Static Hamiltonian

The discussion in this and the following section is based on a paper by Van Kranendonk and Bloom.[2] Since our experiments were done in zero external magnetic field, and since we assume that the hyperfine interaction does not appreciably affect the electron spin system, we can write the Hamiltonian for the electron spins as

$$\mathcal{H}_S = -2J \sum_{i<j} \underline{S}_i \cdot \underline{S}_j \qquad (4.55)$$

where $\underline{S}_i$ is the vector spin operator of the i^{th} electron spin in units of $\hbar$, J is the isotropic coupling constant and is the same for all spins. Equation (4.55) assumes the absence of anisotropy. The total static Hamiltonian $\mathcal{H}_{SS}$ is

$$\mathcal{H}_{SS} = \mathcal{H}_S + \mathcal{H}_U \qquad (4.56)$$

Since we have assumed that $\mathcal{H}_U$ has little effect on the motion of the atomic spins, the electron eigenstates are determined by $\mathcal{H}_S$. Some care must be taken in choosing the eigenstates of $\mathcal{H}_S$ in order that the matrix elements of V are well behaved. Following Van Kranendonk,[2] we represent the eigenstates of $\mathcal{H}_S$ by $|E\alpha)$, where α represents a number of constants of the motion so chosen that for fixed α and α', the matrix elements $(E'\alpha'|\underline{V}|E\alpha)$ are smooth functions of E and E'.

The eigenstates of the total static Hamiltonian $\mathcal{H}_{SS}$ can then be represented by $|E\alpha\pm)$, where the + and -

indicate the relative sign of m, the nuclear spin quantum number. The - sign corresponds to the excited state, while the + sign refers to the ground state.

Two Magnon Relaxation

In Appendix B, Eq. (B-12), it is shown that the relaxation time T_{1n} is given by

$$\frac{1}{T_{1n}} = 2W\downarrow \tag{4.57}$$

where $W\downarrow$ is the probability per unit time that the nuclear spin flips from its excited state to its ground state. Using time dependent perturbation theory[33] the probability per unit time that the nucleus flips, the electron spin system being initially in state $|E\alpha)$, is given by

$$W\downarrow(E\alpha) = \frac{2\pi}{\hbar}\sum_{\alpha'}\int\rho(E'\alpha')|(E'\alpha' + |\mathcal{H}|_V|E\alpha-)|^2\, dE' \tag{4.58}$$

where $\rho(E\alpha)dE$ is the number of states $|E\alpha)$ in energy range dE for a given α. E' is determined by the condition that $E' = E + \hbar\omega_L$ where $\hbar\omega_L$ is the energy given up by the nucleus when dropping from the excited level to the ground state. The electron spins are assumed to be in thermal equilibrium.

The probability per unit time that the nuclear spin flips is then

$$W\downarrow = \overline{W\downarrow(E\alpha)} = \frac{1}{Z}\sum_{\alpha}\int e^{-\beta E}W\downarrow(E\alpha)\rho(E\alpha)dE \tag{4.59}$$

where Z is the partition function

$$Z = \sum_n e^{-\beta E_n} \qquad \beta = \frac{1}{k_B T} \tag{4.60}$$

In the integrand, $\rho(E\alpha)dE$ represents the number of states $|E\alpha)$ for a given α, $e^{-\beta E_n}$ gives the probability that the state $|E\alpha)$ is occupied, and $W\downarrow(E\alpha)$ gives the probability that the nuclear spin flips if the electron system is in $|E\alpha)$.

We are interested in obtaining a theoretical expression for T_{1n} based on the two magnon Raman process discussed earlier. Therefore, considering only those terms $\underline{V}_R$ in $\mathcal{H}_V$ which lead to Raman processes, we have as the perturbation Hamiltonian for Raman processes

$$-\gamma_N \hbar \underline{V}_R \cdot \underline{I} = -\gamma_N \hbar [\tfrac{1}{2}(V_R'^{+} I'^{-} + V_R'^{-} I'^{+}) + V_z' I_z'] \tag{4.61}$$

where $V'^{\pm} = V_x' \pm iV_y'$, and where the prime indicates that the dot product has been evaluated in the (x', y', z') coordinate system in which z' is defined as the direction of the net internal field at the nuclear site and hence is the direction of nuclear quantization. Figure (4.2) shows the relationship between the (x, y, z) and (x', y', z') coordinate system. The z-axis is defined by the direction of the electron magnetization, and has been drawn at an angle θ to the z'-axis. The y'-axis has been drawn in the x-y plane for ease in calculating the perturbation Hamiltonian. The only term

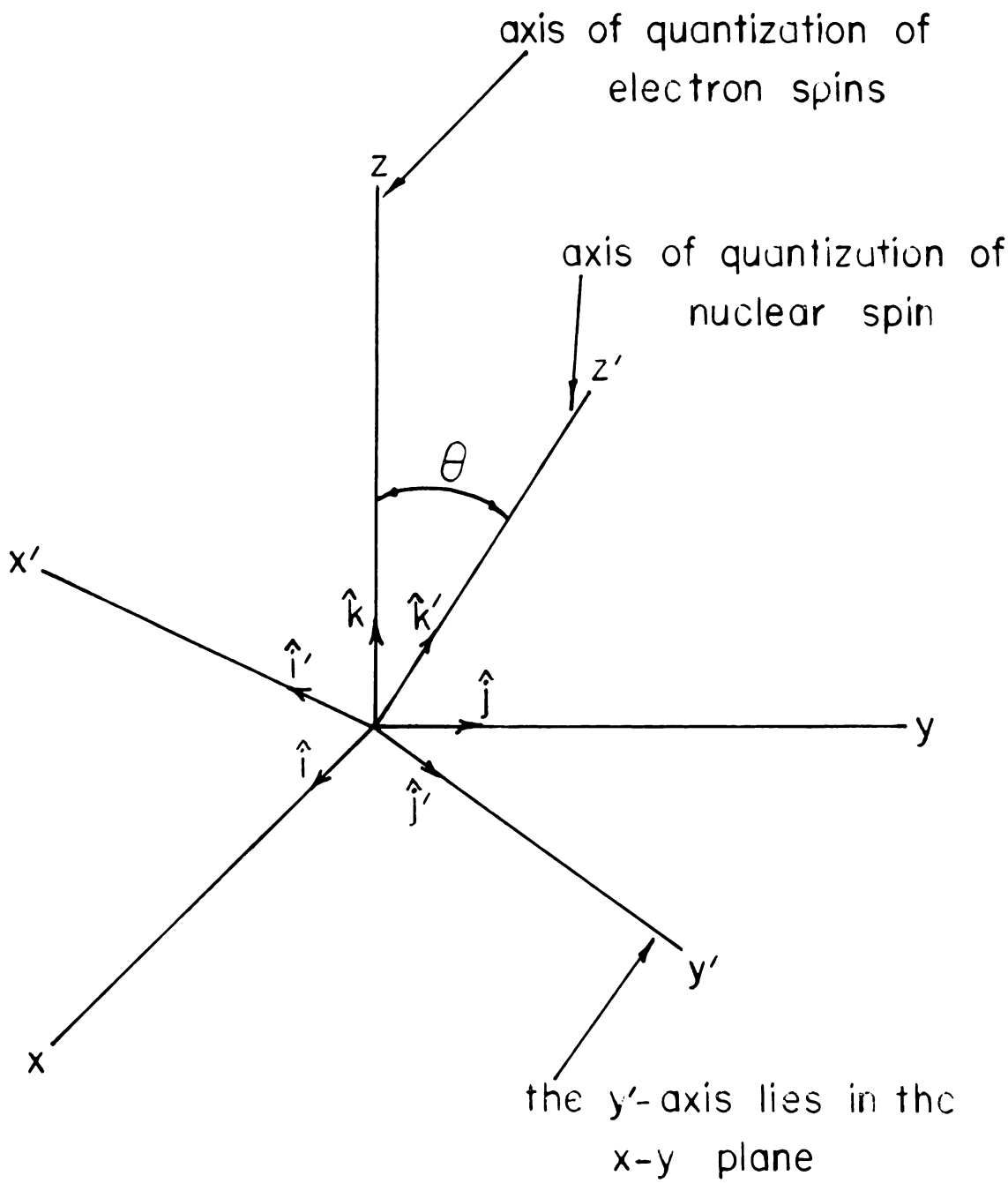

Fig. 4.2. Coordinate systems (x, y, z) and (x', y', z').

in (4.61) that will couple the states $(E'\alpha' +|$ and $|E\alpha -)$ is $\frac{-\gamma_N \hbar}{2} V_R'^{-} I'^{+}$. Therefore the probability per unit time that the nucleus flips due to Raman processes, the electron spin system being initially in state $|E\alpha)$ is, from (4.21),

$$W\downarrow(E\alpha) = \frac{2\pi}{\hbar} \sum_{\alpha'} \int \rho(E'\alpha') |(E'\alpha'+| \mathcal{H}_R'^{-} |E\alpha-)|^2 dE' \qquad (4.62)$$

where

$$\mathcal{H}_R'^{-} = -\tfrac{1}{2}\gamma_N \hbar V_R'^{-} I'^{+} \qquad (4.63)$$

To write down the explicit form for $V_R'^{-}$, it is necessary to recall that only fluctuations in the z-component of $\underline{S}$ contribute to two magnon processes. We therefore take δS_x and δS_y to be zero. Then, from Eq. (4.53) we can write

$$V_R'^{-} = \sum_i d_i [\delta S_i'^{-} - \frac{3}{r_i^2} (\delta S_{iz} r_{iz}) r_i'^{-}] \qquad (4.64)$$

Since the transformation to magnon operators is generally written in the (x, y, z) coordinate system, we express $\delta S_i'^{-}$ in this system. Then

$$\delta S_{ix}' = \hat{i}' \cdot \hat{k} \delta S_{iz} = \delta S_{iz} \sin\theta \qquad (4.65)$$

$$\delta S_{iy}' = \hat{j}' \cdot \hat{k} \delta S_{iz} = \delta S_{iz}(0) = 0 \qquad (4.66)$$

$$\delta S_i'^{-} = \delta S_{ix}' - i\delta S_{iy}' = \delta S_{iz} \sin\theta \qquad (4.67)$$

Then $V_R'^-$ can be written

$$V_R'^- = \sum_i d_i[\sin\theta - \frac{3}{r_i^2}(r_{iz})r_i'^-]\delta S_{iz} \qquad (4.68)$$

δS_{iz} is easily expressed in terms of magnon creation and annihilation operators by substituting the expectation values of the operators S^z_{qj} and S^z_{rj} (Eqs. (4.42) and (4.43)) into Eq. (4.54). However not all two magnon terms in (4.42) and (4.43) are Raman terms. If we consider only those terms which have the Raman form $A^+_{kp}A_{kp}$, then for the two sublattices we have

$$\delta S^z_{qj} = \left(\frac{2}{N}\right)\sum_{kk'} e^{i(\underline{k}-\underline{k}')\cdot\underline{r}_j}(c_{k1}c_{k'1}A^+_{k1}A_{k'1} + c_{k2}c_{k'2}A^+_{k'2}A_{k2}) \qquad (4.69)$$

$$\delta S^z_{rj} = -\left(\frac{2}{N}\right)\sum_{kk'} e^{-i(\underline{k}-\underline{k}')\cdot\underline{r}_\ell}(c_{k2}c_{k'2}A^+_{k'1}A_{k1} + c_{k1}c_{k'1}A^+_{kz}A_{k'z}) \qquad (4.70)$$

where we have used the fact the $[A_{kp},A_{k'p}] = 0$ for $k \neq k'$. Using (4.69) and (4.70) in (4.68) we can write $V_R'^-$ as

$$V_R'^- = \left(\frac{2}{N}\right)\sum_{\substack{k,k' \\ k\neq k'}}(d_{kk'1}A^+_{k1}A_{k'1} + d^*_{kk';2}A^+_{k2}A_{k'2}) \qquad (4.71)$$

where

$$d_{kk';p} = D'(\underline{k}-\underline{k}')c_{kp}c_{k'p} - D''(\underline{k}-\underline{k}')c_{k,3-p}c_{k';3-p} \qquad (4.72)$$

$$D'(\underline{k}) = \sum_i D_i \exp(i\underline{k}\cdot\underline{r}_i); \quad D''(\underline{k}) = \sum_j D_j \exp(i\underline{k}\cdot\underline{r}_j) \tag{4.73}$$

$$D_i = -(\gamma_e \hbar / r_i^3)\left[\sin\theta - \left(\frac{3}{r_i^2}\right) z_i (x_i' - i y_i')\right] \tag{4.74}$$

and where p represents the polarization mode of the magnons, p = 1,2, and * means complex conjugate. The fact that k and k' in (4.69) and (4.70) are dummy indices and can be interchanged has been used in deriving (4.71). Using (4.63) in (4.62) gives

$$W\downarrow(E\alpha) = \frac{\pi}{2\hbar}\gamma_N^2 \hbar^2 \sum_{\alpha'} \int \rho(E'\alpha') |(E'\alpha'|V_R'^-|E\alpha)|^2 dE' \tag{4.75}$$

To calculate $W\downarrow(E\alpha)$ we evaluate $(E'\alpha'|V_R'^-|E\alpha)$ for particular initial and final states using (4.71) and then sum over all allowable final states. Suppose that in the Raman process a magnon $\underline{k}p'$ is absorbed and a magnon $\underline{k}'p'$ is emitted. Let the final state $|E'\alpha')$ be represented by $|E', \hat{n}'_{mp}, d\Omega', p')$, by which we mean there are $\hat{n}'_{mp}$ magnons present in the mode $\underline{m}p$, where $\underline{m}$ runs over the $\frac{1}{2}N$ wave vectors and p = 1,2, plus one additional magnon of polarization p' and wavevector $\underline{k}'$ lying in the solid angle $d\Omega'$. Here $\hat{n}'_{mp} = n_{mp} - \delta_{ml}\delta_{pp'}$. The initial state $|E\alpha)$ is then $|E, n_{mp})$. The length of $\underline{k}'$ must be such that energy is conserved, so $E' = E + \hbar\omega_L$. Since E and E' are generally much larger than $\hbar\omega_L$, we may set E' = E when making calculations. Recalling that

$$A_k^+|\ldots n_k \ldots) = (n_k + 1)^{\frac{1}{2}}|\ldots n_k + 1 \ldots) \tag{4.76}$$

and

$$A_k|\ldots n_k\ldots) = (n_k)^{\frac{1}{2}}|\ldots n_k-1\ldots) \tag{4.77}$$

Eq. (4.75) becomes

$$W\downarrow(E\alpha) = \frac{2\pi\gamma_N^2\hbar}{N^2}\sum_{\alpha'}\rho(E'\alpha')(n_{kp'}+1)(n_{k'p'})\left|d_{kk';p'}\right|^2 \tag{4.78}$$

where the sum over α' involves an integration over $d\Omega_k$ and a summation over modes $\underline{k}'p'$, where k' ranges over the $\frac{N}{2}$ values in the first Brillouin zone. The density of states for fixed α is given by Appendix C

$$\rho(E\alpha) = \frac{V}{8\pi^3}f(\underline{k},p)k^2d\Omega_k \tag{4.79}$$

where $f(\underline{k},p) = |\partial\hbar\omega_{kp}/\partial\underline{k}|^{-1}$. With Van Kranendonk we assume that $f(\underline{k},p)$ is independent of p and the direction of $\underline{k}$, and that the first Brillouin zone can be replaced by a sphere of radius k_m such that

$$\frac{V}{2\pi^2}\int_o^{k_m}k^2dk = \frac{N}{2} \tag{4.80}$$

The latter assumption, in conjunction with the use of E = E', means that we can set k = k'. Then (4.78) becomes, using (4.79), summing over $\underline{k}'p'$ and integrating over $d\Omega_k$,

$$W\downarrow(E\alpha) = \frac{2\pi\gamma_N^2\hbar}{N^2}\ (4\pi)\sum_{p'}\ \sum_{k'}\frac{V}{8\pi^3}f(k)k^2$$

$$\times(n_{kp'}+1)(n_{kp'})\left|d_{kk',p'}\right|^2 \tag{4.81}$$

or

$$W\downarrow(E\alpha) = \frac{v^2\gamma_N^2\hbar}{2\pi^3}\sum_p\int_o^{k_m} f(k)k^4(n_{kp}+1)(n_{kp})\{|d_{kk',p}|^2\}dk \quad (4.82)$$

where $v = (V/N)$ and the curly brackets mean that $|d_{kk',p}|^2$ should be averaged over all directions $\underline{k}$ and $\underline{k}'$.

The total transition probability $W\downarrow$ is equal to the average of (4.81) over all initial states $|E\alpha)$. Therefore

$$W\downarrow = \frac{v^2\gamma_N^2\hbar}{2\pi^3}\sum_p\int_o^{k_m} f(k)k^4(\bar{n}_{kp}+1)(\bar{n}_{kp})\{|d_{kk',p}|^2\}dk \quad (4.83)$$

where $\bar{n}_{kp}$ is the average value of the population of magnons in mode $\underline{k}p$. For non-interacting magnons this is given by the boson occupation number,

$$\bar{n}_{kp} = (e^x-1)^{-1};\ x = \hbar\omega_{kp}/k_BT \quad (4.84)$$

At temperatures low enough that only long wavelength magnons are excited, the following approximations can be made, where we assume $(\omega_A/\omega_e)^2 << (\omega_A/\omega_e) << 1$.

$$\hbar\omega_{kp} = \omega_e(bk^2 + \frac{2\omega_A}{\omega_e})^{\frac{1}{2}} \quad (4.85)$$

$$c_{k1}{}^2 = c_{k2}{}^2 = \tfrac{1}{2}(bk^2 + \frac{2\omega_A}{\omega_e})^{-\frac{1}{2}} \quad (4.86)$$

$$d_{kk;p} = Dc_{kp}{}^2;\quad D = \sum_i D_i - \sum_j D_j \quad (4.87)$$

Using Eqs. (4.84) through (4.87) in (4.83) gives, after

changing variables from k to x and performing an integration by parts,

$$W\downarrow = KT^3\int_{T_{AE}/T}^{\infty} x(e^x-1)^{-1}dx \tag{4.88}$$

where $x = \hbar\omega_k/k_BT$,

$$K = \frac{1}{T_N^3}\left(\frac{6}{\pi^2}\right)\frac{\eta^4(S+1)^4v^2|D|^2\gamma_N^2\hbar}{(4)3^5\pi b^3k_BT_N} \tag{4.89}$$

and

$$\eta = \frac{3k_BT_N}{2JS(S+1)z} \tag{4.90}$$

The relaxation time may then be found from Eq. (4.57) giving

$$\frac{1}{T_{1n}} = 2KT^3\int_{T_{AE}/T}^{\infty} x(e^x-1)^{-1}dx \tag{4.91}$$

For large values of T, the lower limit approaches zero and the integral approaches a constant, $\pi^2/6$. The temperature dependence of T_{1n} is then given by

$$T_1^{-1} \propto T^3 \tag{4.92}$$

for $T >> T_{AE}$.

V. EXPERIMENTAL RESULTS AND DISCUSSION

Rubidium Manganese Chloride di-hydrate ($Rb_2MnCl_4 \cdot 2H_2O$) is a triclinic crystal with space group $P\bar{1}$[34] which becomes antiferromagnetically ordered below $T_N = 2.24°K$.[35] The internal fields are of such magnitude that nuclear magnetic resonance experiments can be readily performed on four nuclei, Rb^{85}, Rb^{87}, Cl^{35} and H^1. We have measured T_{1n}, the nuclear spin-lattice relaxation time, as a function of temperature for these four nuclei in the temperature range from 1.6°K to 0.45°K and in one instance, for Rb^{87}, to 0.32°K. Table 5.1 shows the frequencies (at 1.1°K) of the lines studied, together with the magnitude and type of the corresponding internal magnetic fields.[36] These lines were chosen for detailed study because of their good signal to noise ratios. Less extensive data on other lines showed the same temperature dependence of T_{1n}. All measurements were made in zero external magnetic field, using the standard pulse techniques discussed in Chapter II.

Temperature Dependence of T_{1n}

The results are shown in Figures 5.1 through 5.5,

Table 5.1 Information on frequencies and magnetic fields for resonance lines studied.

Nucleus	Freq. at 1.1°K MHz	Magnitude of Internal Field (Oersteds)	Type
Rb^{87}	3.89	1.879	dipolar
Rb^{85}	3.22	1.879	dipolar
Cl^{35}	8.53	19.49	transferred hyperfine
H^{1}	18.1	4.296	dipolar

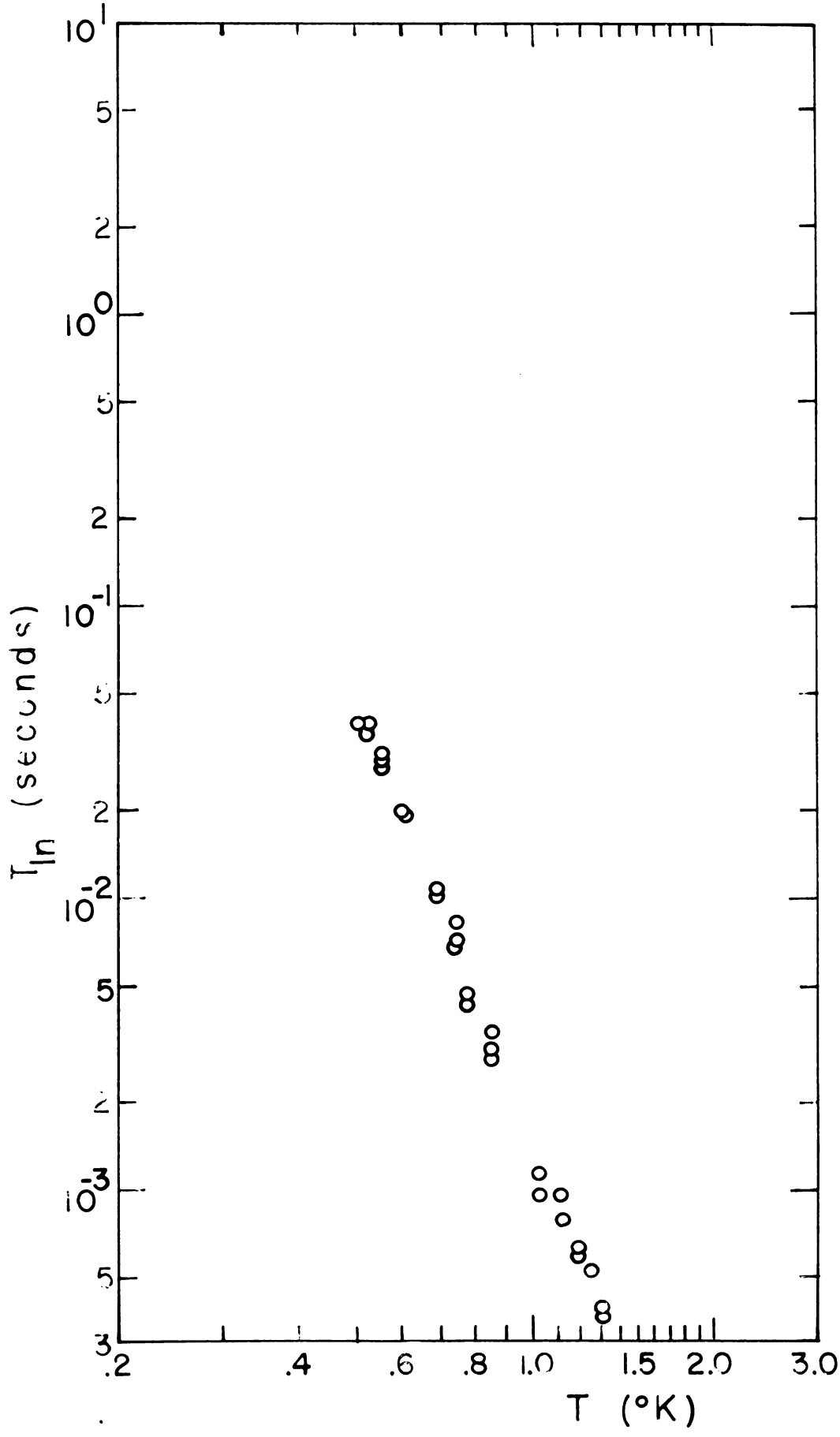

Fig. 5.1. Graph of T_{1n} vs. T for F^{19}.

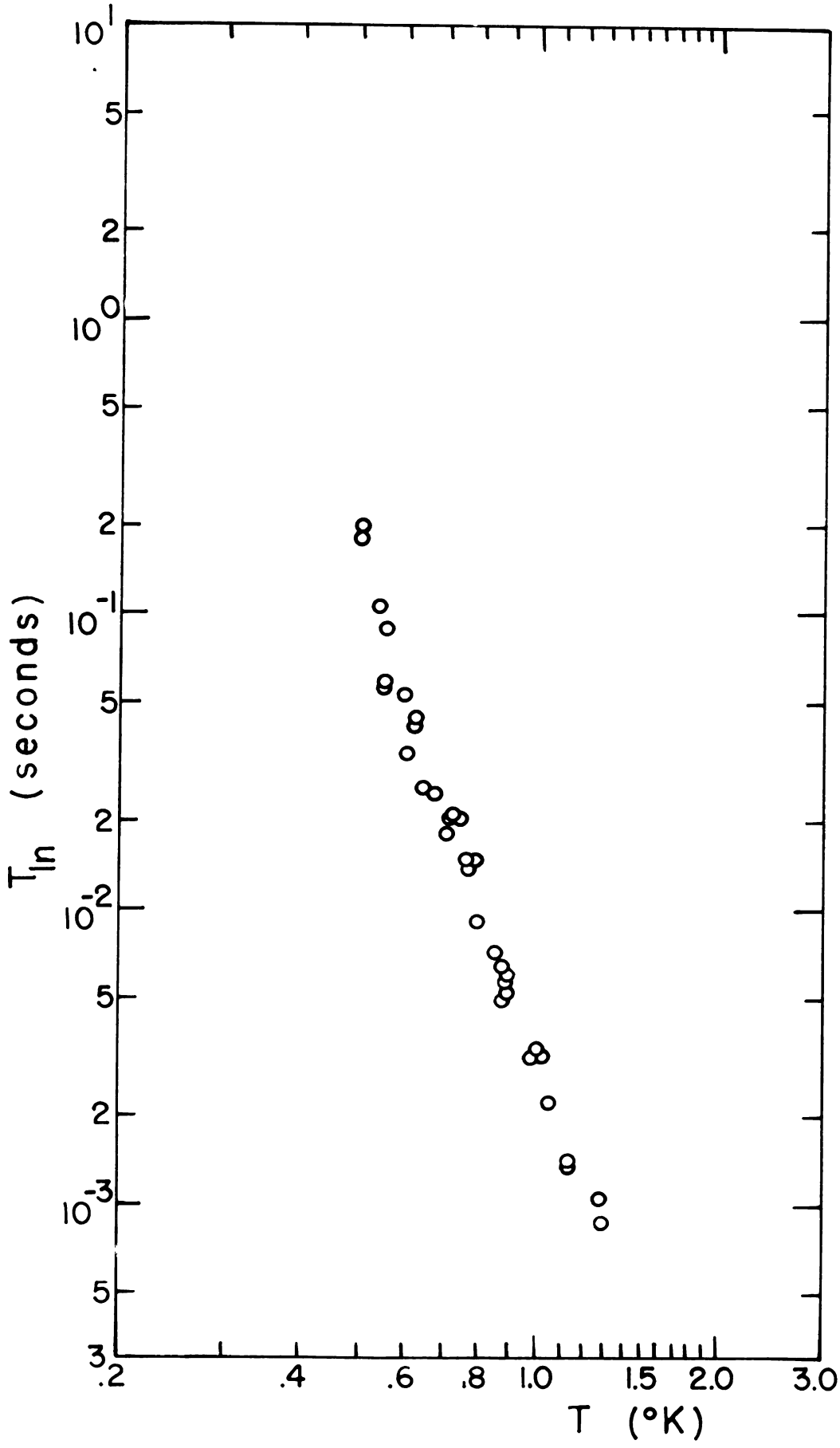

Fig. 5.2. Graph of T_{ln} vs. T for Cl^{35}.

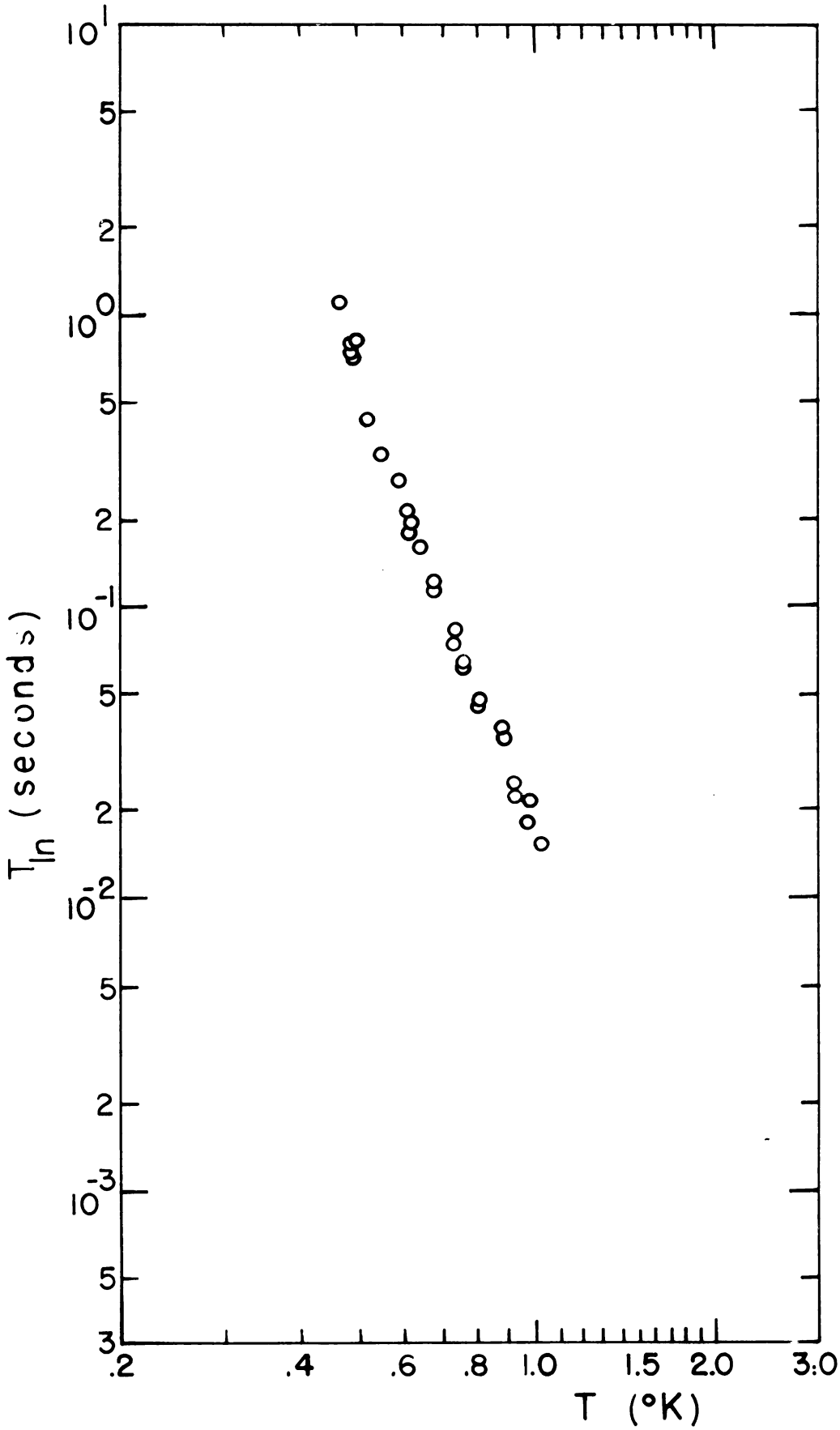

Fig. 5.3. Graph of T_{1n} vs. T for Rb^{85}.

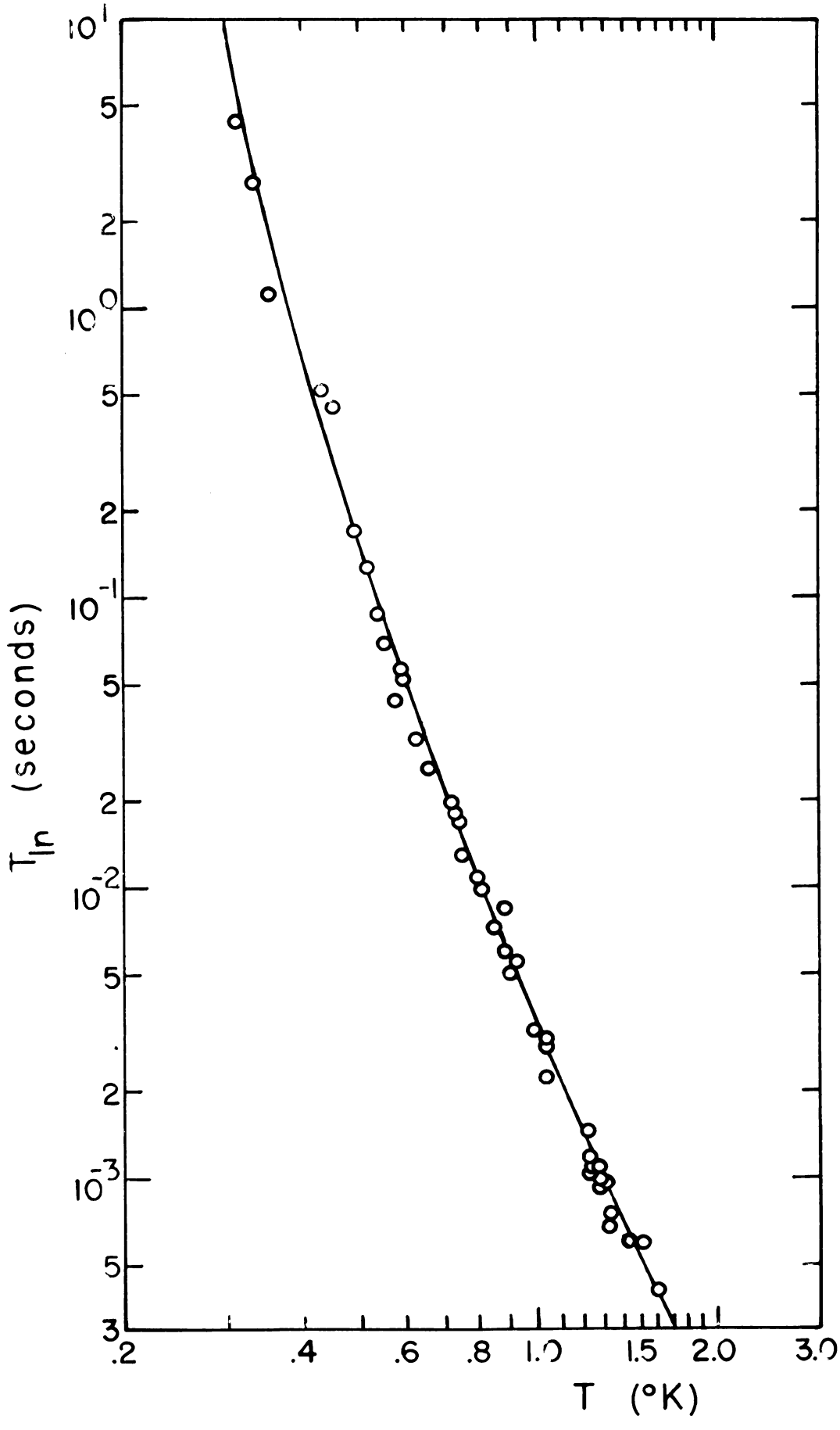

Fig. 5.4. Graph of T_{in} vs. T for Rb^{87}.

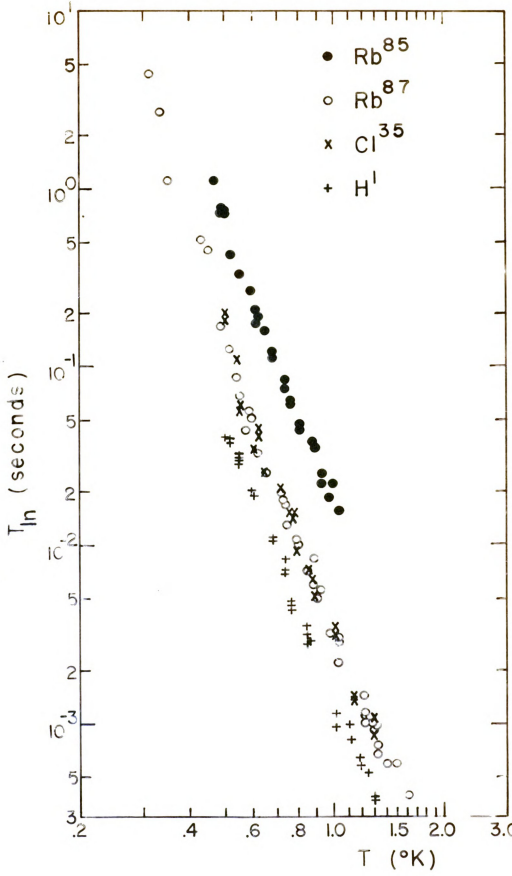

Fig. 5.5. Graph of T_{1n} vs. T for H^1, Cl^{35}, Rb^{85}, and Rb^{87}.

where T_{1n} is plotted vs. T on log-log paper. Although the electric quadrupole moments of Cl^{35}, Rb^{87} and Rb^{85} differ by a factor of four, the temperature dependence of their relaxation times appears to be the same (Fig. 5.5) and further, is the same as that for the proton, which has no quadrupole moment. Therefore, we will neglect the effects of the quadrupole interaction, and, in the initial discussion of the results, will consider only the Rb^{87} relaxation, for which the data is the most extensive.

The theoretical expression for T_{1n} derived in Chapter IV for Raman relaxation resulted in $T_{1n} \propto T^{-3}$ for $T >> T_{AE}$. Similar calculations based on three-magnon relaxation processes[37] lead to $T_{1n} \propto T^{-5}$ for $T >> T_{AE}$. If relaxation occurred via one of these processes, and if T were much greater than T_{AE}, a graph of log T_{1n} vs. log T would be a straight line of slope -3 or -5. Evidence of such temperature dependences above T_{AE} does exist in other crystals.[38,39] However, the data for Rb^{87} in Fig. 5.4 clearly cannot be fit by a single straight line. This suggests that we are studying a temperature range where magnon energy gap effects are important.

The size of the energy gap in the magnon dispersion relation can be calculated from the value of the experimentally determined critical field, H_c, required to produce the spin-flop phenomenon.[40] The calculation

is based on the relation[41]

$$k_B T_{AE} = g\mu_o H_c = g\mu_o (2H_E H_A + H_A^2)^{\frac{1}{2}} \qquad (5.1)$$

where

$$g\mu_o H_E = \hbar\omega_e \qquad g\mu_o H_A = \hbar\omega_A \qquad (5.2)$$

An estimate of H_E can be obtained from the approximate relation

$$g\mu_o H_E \simeq k_B T_N \qquad (5.3)$$

Measurements by Casey, Nagarajan, and Spence[42] in $Rb_2MnCl_4 \cdot 2H_2O$ show no critical field effects below 8.3 kgauss at 1.1°K, which sets a lower limit on H_c. Thus from (5.1) we have $T_{AE} \geq 1.1°K$. Blatt, Butterworth and Abele[43] searched for critical field effects in the same crystal using thermal detection methods. They found no evidence of a spin-flop phase above about 1.2°K, though they did detect an antiferromagnetic-paramagnetic phase transition at about 18 kgauss. Although measurements at lower temperatures may detect a spin-flop transition, an estimate of T_{AE} based on their existing data gives $T_{AE} \simeq T_N$.

Another estimate of T_{AE} can be made by comparison with $MnCl_2 \cdot 4H_2O$, which exhibits a magnetization curve very similar to that of $Rb_2MnCl_4 \cdot 2H_2O$. Figure 5.6 plots (M/M_o) vs. (T/T_N) for $MnCl_2 \cdot 4H_2O$[44] and

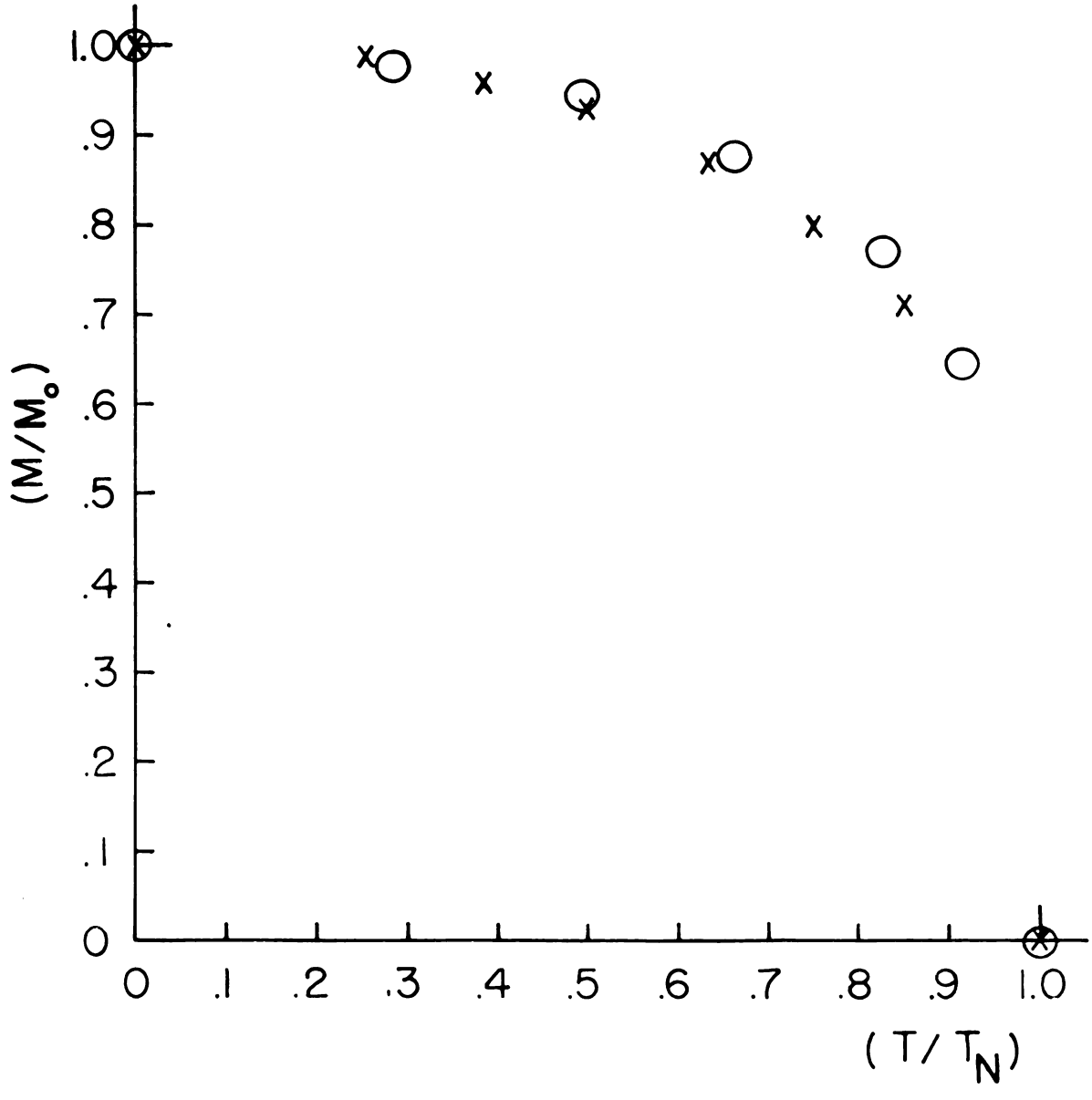

Fig. 5.6. Magnetization curves for $MnCl_2 \cdot 4H_2O$ and $Rb_2MnCl_4 \cdot 2H_2O$.

$Rb_2MnCl_4 \cdot 2H_2O$.[45] The shape of the magnetization curve is related to T_{AE} since the ratio of M(T) to M_o will depend on the number of magnons present at temperature T. In $MnCl_2 \cdot 4H_2O$, $T_{AE} \simeq .8T_N$;[46] we therefore might expect $T_{AE} \simeq 1.8°K$ for $Rb_2MnCl_4 \cdot 2H_2O$.

The three estimates of T_{AE} cited above suggest that there is a large energy gap in the magnon spectrum which supports our qualitative conclusions from the shape of the curve in Fig. 5.4.

In order to compare the temperature dependence of T_{1n} with theory we must determine the relaxation mechanism. As discussed in Chapter IV, the presence of a large gap eliminates direct and three-magnon processes, leaving the two magnon Raman process as the dominant intrinsic relaxation mechanism. There is the possibility that the relaxation is not intrinsic, but occurs via a paramagnetic impurity. We believe, however, that the measured T_{1n}'s are intrinsic for the following reason. As the temperature is lowered, electron relaxation times, T_{1e}, of almost all measured ions[47] become proportional to T^{-1} above 1°K and in general[48] $T_{1n} \propto T_{1e}^{\alpha}$ where α is between 0.25 and 1. Therefore, if impurity relaxation were dominant in our experiments, the steep temperature dependence of T_{1n} for Rb^{87} down to 0.32°K would not be observed.

The theoretical temperature dependence of T_{1n}

for Raman relaxation in the small k approximation is, from (4.88),

$$\frac{1}{T_{1n}} = 2KT^3 \int_{T_{AE}/T}^{\infty} x(e^x-1)^{-1}dx \qquad (5.4)$$

where

$$K = \frac{1}{T_N^3} \frac{6\eta^4(S+1)^4 v^2 |D|^2 \gamma_N^2 \hbar}{4\pi^3(3^5)b^3 k_B T_N} \qquad (5.5)$$

A least squares fit of the Rb^{87} data to (5.4) for various values of T_{AE} gave $T_{AE} = 2.36°K$. The solid line in Fig. 5.4 represents the theoretical T_{1n} for this value of T_{AE}. Similar fits to the other three nuclei gave optimum T_{AE}'s within ±10% of this value, as shown in Table 5.2. It is emphasized that the values of K given in Table 5.2 were determined by fitting (5.4) to the data, and were not evaluated from (5.5).

Calculated Values of T_{1n}

A calculation of the order of magnitude of K in the small k approximation involves estimates of the parameters η, v, b and D in (5.5). It is easiest to calculate K for the proton for two reasons. First, the internal field at the proton site is largely determined by the nearest neighbor Mn ion which simplifies the calculation of D. Second, the proton has no quadrupole moment, so that quadrupole effects do not influence the observed T_{1n} and the free ion γ_N can be used

Table 5.2. Results of least squares fit to equation (5.4) for the four nuclei studied

Nucleus	Spin	$2K(sec^{-1}(°K)^{-3})$	$T_{AE}(°K)$
H^{1}	1/2	1.96×10^{3}	2.15
Cl^{35}	3/2	1.08×10^{3}	2.47
Rb^{87}	3/2	0.973×10^{3}	2.36
Rb^{85}	5/2	0.133×10^{3}	2.04

in the calculations. We calculate below a numerical value for 2K for the proton site studied. In the molecular field approximation $\eta = 1$, but in higher order approximation[49] it is a function of S, z and lattice topology such that η varies between extremes of 0.68 and 0.86. Based on this we take $\eta = 0.8$. Following Van Kranendonk[50] and Moriya[51] we take $b = \frac{1}{3}v^{2/3}$. Neglecting the effect of all but the nearest neighbor Mn ion, we find D to be $1.61 \times 10^{3}\,\mathrm{erg(oe)^{-1}cm^{-3}}$ when the internal field makes an angle of 10° to the magnetization and have used $r_i = 2.72\text{Å}$.[52] The Mn ground state has S = 5/2, and γ_N for protons is $2.7 \times 10^{4}\ \mathrm{sec^{-1}oe^{-1}}$. These estimates give $2K = .037 \times 10^{3}\ \mathrm{sec^{-1}(°K)^{-3}}$. This is too small by a factor of about 50, making the calculated T_{1n} too long by the same factor.

There are two reasons why T_{1n} determined by the small k approximation is too long. In discussing these it will be useful to consider Eq. (4.83) which is rewritten below

$$W\downarrow = \frac{v^2\gamma_N{}^2h}{2\pi^3}\sum_p\int_o^{k_m} f(k)k^4(\bar{n}_{kp}+1)(\bar{n}_{kp})\{|d_{kk',p}|^2\}dk \qquad (5.6)$$

First, we have assumed a linear spin wave theory in which spin waves do not interact. If one considers interacting magnons, it is found that it is easier to create a magnon if there is already one present. Taking this into account, a renormalization of the

energy $\hbar\omega_k$ must be made,[53] with the result that the number of spin waves at a given temperature increases. This in turn increases the transition probability and lowers T_{1n}.

Second, the small k approximation with $\frac{\omega_A}{\omega_e} << 1$ leads to an expression for ω_k such that for $k \simeq k_m$, the integrand in (5.6) is so small that extension of the upper limit of integration from k_m to infinity does not affect the value of the integral. However, for appreciable anisotropy, this is not the case, for reasons discussed below.

The following calculation of T_{1n} is an attempt to remedy the defects in the small k approximation within the framework of a linear spin wave theory. We start from Eq. (5.6). It is necessary to obtain expressions for ω_k, $f(k)$, γ_k and c_k. First, approximate the dispersion curve by a straight line such that (Fig. 5.7)

$$\hbar\omega_k = \frac{ak_B(T_N - T_{AE})}{\pi} k + k_B T_A \qquad (5.7)$$

Then

$$f(k) = \frac{\pi}{ak_B(T_N - T_{AE})} \qquad (5.8)$$

Second, notice that γ_k defined by (4.22) has a maximum value of one. γ_k carries the k dependence of c_{k1} and c_{k2} which are needed in determining $|d_{kk';p}|^2$. Taking as T_{AE} the value 1.8°K determined earlier by comparison

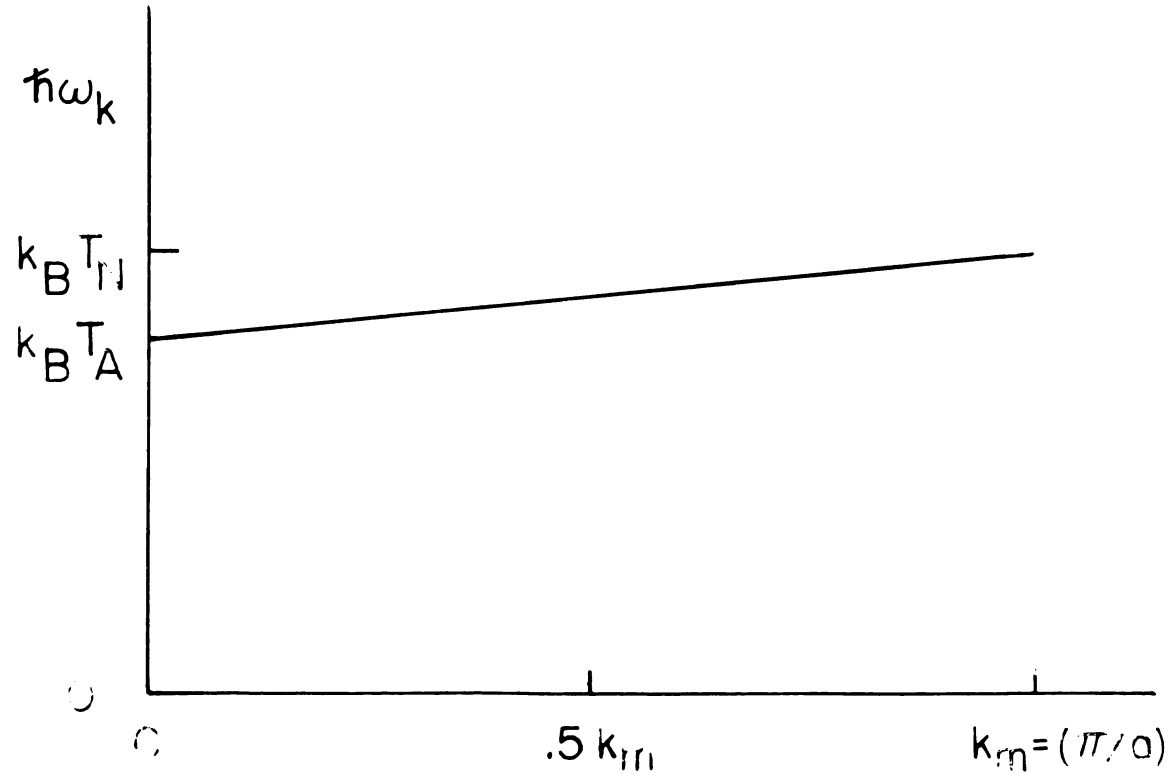

Fig. 5.7. Hypothetical dispersion curve for magnons in antiferromagnet with large anisotropy field. Equation of straight line is $\omega_k = [ak_B(T_N - T_{AE})/\pi\hbar]\, k + (k_B T_{AE}/\hbar)$.

with $MnCl_2 \cdot 4H_2O$, and using (5.1) through (5.3) we find $\frac{\omega_A}{\omega_e} \simeq .4$. Now c_{k1}, c_{k2} and ρ_k are defined by (4.29) and (4.30)

$$c_{k1} = \frac{\rho_k}{(\rho_k^2 - \gamma_k^2)^{\frac{1}{2}}} \qquad c_{k2} = \frac{-\gamma_k}{(\rho_k^2 - \gamma_k^2)^{\frac{1}{2}}} \tag{5.9}$$

$$\rho_k = 1 + \frac{\omega_A}{\omega_e} + [(1 + \frac{\omega_A}{\omega_e})^2 - \gamma_k^2]^{\frac{1}{2}} \tag{5.10}$$

Using $(\omega_A/\omega_e) = .4$, we find that ρ_k for $\gamma_k = 1$ is less than 20% smaller than ρ_k for $\gamma_k = 0$. Since we are interested only in order of magnitude estimates, let $\gamma_k = 0$. Then $c_{k2} = 0$ and $c_{k1} = 1$, and in the determination of $d_{kk';p}$ we will have only one term. The result is that

$$|d_{kk';1}|^2 = D_i^2 = D^2 \tag{5.11}$$

Eq. (5.6) then becomes

$$W\downarrow = \frac{v^2\gamma_N^2\hbar}{2\pi^3} \int_o^{k_m} \frac{k^4\pi}{ak_B(T_N - T_A)} \frac{e^x}{(e^x-1)^2} D^2 dk \tag{5.12}$$

where $x = \hbar\omega_k/k_BT$. Changing variables from k to x gives

$$W = \frac{v^2\gamma_N^2\hbar\pi^6D^2}{2\pi^3a^2k_B(T_N-T_{AE})^6}T^5\int_{T_{AE}/T}^{T_N/T}(x-x_g)^4\frac{e^x}{(e^x-1)^2}\,dx \tag{5.13}$$

This expression makes no restrictions on k, and it can be shown that the integrand is far from negligible at $x = \frac{T_N}{T}$. At T = 1°K, numerical integration of (5.13)

gives $W\downarrow \simeq 2 \times 10^2 sec^{-1}$, so $T_{1n} \simeq 2.5$ msec. The degree of agreement with our measured value of 1.75 msec is probably fortuitous, and the above calculation is meant simply to indicate that large k magnons cannot be neglected when the slope of the dispersion curve is small.

As a check on the validity of the temperature dependence of (5.13), $W\downarrow$ was calculated for T = .5°K. The result was $W\downarrow = 16.6\ sec^{-1}$ which gave $T_{1n} \simeq 30$ msec again in close agreement with the experimental value of 40 msec.

A calculation of T_{1n} for Rb^{87} and Rb^{85} is more difficult, because the internal field at the rubidium site is not dominated by one Mn ion, as it was for H^1, but is determined by three or four neighboring Mn ions.[54] Any estimate of D would be more approximate than the calculation of D for protons and no such estimate has been made. However, since Rb^{85} and Rb^{87} occupy the same crystallographic site, we can attempt to explain the difference in the T_{1n} values for the two nuclei. Neglecting quadrupole effects, this difference arises from the γ_N^2 factor in Eq. (5.5). The nucleus with larger γ_N (Rb^{87}) will relax faster. Qualitatively this is seen to be the case. To make a quantitative determination of T_{1n} it is necessary to determine an effective γ_N for each isotope.

Relaxation at the Cl^{35} sites occurs through fluctuations in the transferred hyperfine interaction,

$\mathcal{H}_{IS} = \underline{I}\cdot\underline{\underline{A}}\cdot\underline{S}$ where A is the hyperfine tensor. Since the internal field at the Cl^{35} sites is essentially parallel to the magnetization direction, the (x, y, z) and (x', y', z') coordinate systems are identical. The terms in $\underline{\underline{A}}$ which couple I_x and I_y to fluctuations in S_z are the anisotropic terms A_{xz} and A_{yz}. The Hamiltonian which induces nuclear transitions from the excited state to the ground state via two magnon Raman terms can be obtained from

$$\mathcal{H}_{IS} = \tfrac{1}{2}(A_{xz} - iA_{yz})\delta S^z I^+ \qquad (5.14)$$

using Eqs. (4.69) and (4.70). Taking the resultant expression as the perturbation Hamiltonian in (4.62) we can derive an expression for T_{1n} based on the transferred hyperfine interaction. However, we have no experimental values for the terms A_{xz} and A_{yz}, and so cannot make a quantitative estimate of T_{1n} for Cl^{35}.

Conclusions

The measurements of T_{1n} vs. T in antiferromagnetic $Rb_2MnCl_4\cdot 2H_2O$ suggest the following qualitative conclusions. First, the relaxation occurs via a two magnon Raman relaxation mechanism and is not due to impurity relaxation processes. Second, there is evidence that T_{1n} is being affected by a large energy gap $k_B T_{AE}$ in the magnon spectrum since the plot of log T_{1n} vs. log T

is not a straight line, and a large energy gap does indeed introduce an exponential dependence in the theoretical expression for T_{1n}. Third, since the qualitative temperature dependence of T_{1n} is the same for quadrupolar and non-quadrupolar nuclei, the effect of the quadrupole moment on the temperature dependence of T_{1n} is not critical. Finally, it has been shown that when the dispersion curve is relatively flat, the effect of high k magnons is important.

Several areas of interest are open for further experiment. Measurements of T_{1n} for nuclei in an antiferromagnet where $\omega_A << \omega_e$ would allow better comparison with theory. Preliminary measurements of proton T_1's in $CsMnCl_3 \cdot 2H_2O$, which might satisfy this requirement, indicate $T_{1n} \propto T^{-4.5}$. No attempt has yet been made to measure Cl^{35} relaxation rates in this crystal.

Because values of H_A and T_{AE} are well known for $MnCl_2 \cdot 4H_2O$, measurements of T_{1n} for H^1 and Cl^{35} in this crystal would permit a more accurate check on the theoretical expressions for T_{1n} and would help in the interpretation of data in $Rb_2MnCl_4 \cdot 2H_2O$.

REFERENCES

REFERENCES

1. G. E. G. Hardeman, N. J. Poulis, and W. Van der Lugt, Physica XXII, 48 (1956).

2. J. Van Kranendonk and M. Bloom, Physica XXII, 545 (1956).

3. P. W. Anderson, Phys. Rev. 86, 694 (1952).

4. T. Moriya, Progr. Theoret. Phys. (Kyoto) 16, 23 (1956).

5. C. P. Slichter, Principles of Magnetic Resonance (Harper and Row, New York, 1963), p. 2.

6. Ibid., p. 15.

7. A. Abragam, The Principles of Nuclear Magnetism (Oxford: Clarendon Press, 1961), p. 2.

8. T. P. Das and E. L. Hahn, Solid State Physics (F. Seitz and D. Turnbull, eds., Academic Press, Inc., New York, 1958), Supplement 1, p. 5.

9. A. Abragam, op. cit., p. 44.

10. J. Van Kranendonk and M. Bloom, op. cit., p. 546.

11. Ibid., p. 547.

12. Ibid., p. 546.

13. E. L. Hahn, Phys. Rev. 80, 580 (1950).

14. H. Y. Carr and E. M. Purcell, Phys. Rev. 94, 630 (1954).

15. I. J. Lowe and R. E. Norberg, Phys. Rev. 107, 46 (1957).

16. C. P. Slichter, op. cit., p. 20.

17. A. Narath, Hyperfine Interactions (A. Freeman and R. Frankel, eds., Academic Press, Inc., New York, 1967), p. 297.

18. A. Abragam, op. cit., p. 157.

19. J. A. Cowen, R. D. Spence, H. VanTill, and H. Weinstock, Rev. Sci. Instr. 35, 914 (1964).

20. The susceptibility coils were a smaller version of those described by H. VanTill, Ph.D. Thesis, Michigan State University (1965), Chapter I.

21. D. Lancaster, Popular Electronics, (Sept., 1965), p. 60.

22. J. J. Skopas, Rev. Sci. Instr. 36, 1436 (1965).

23. A. Narath, op. cit., p. 300.

24. V. Jaccarino, Magnetism (G. T. Rado and H. Suhl, eds., Academic Press, Inc., New York, 1963), Vol. IIA, p. 316.

25. Ibid., p. 348.

26. J. Van Kranendonk and J. H. Van Vleck, Revs. Mod. Phys. 30, 1 (1958).

27. C. Kittel, Quantum Theory of Solids (John Wiley and Sons, Inc., New York, 1963), p. 58.

28. Idem.

29. T. Holstein and H. Primakoff, Phys. Rev. 58, 1098 (1940).

30. C. Kittel, op. cit., p. 51.

31. D. C. Mattis, The Theory of Magnetism (Harper and Row, New York, 1965), p. 153.

32. A. Narath, op. cit., p. 325.

33. L. I. Schiff, Quantum Mechanics (McGraw Hill Book Company, Inc., New York, Second Edition, 1955), p. 199.

34. S. J. Jensen, Acta Chem. Scand. 18, 2085 (1964).

35. H. Forstat, N. D. Love, and J. N. McElearney, private communication.

36. J. A. Casey, Ph.D. Thesis, Michigan State University (1967).

37. L. B. Welsh, Ph.D. Thesis, University of California, Berkeley, (1966).

38. Idem.

39. N. Kaplan, R. Louden, V. Jaccarino, H. J. Guggenheim, D. Beeman, and P. A. Pincus, Phys. Rev. Letters, 17, 357 (1966).

40. A. H. Morrish, The Physical Principles of Magnetism (John Wiley and Sons, Inc., New York, 1965), p. 475.

41. Ibid., p. 616.

42. J. A. Casey, op. cit.

43. J. Butterworth, private communication.

44. R. D. Spence and V. Nagarajan, Phys. Rev. 149, 191 (1966).

45. R. D. Spence, private communication.

46. J. Rives, private communication.

47. C. D. Jeffries, Dynamic Nuclear Orientation (J. Wiley and Sons, Inc., New York, 1963), chapter 3.

48. Ibid., p. 77.

49. J. Van Kranendonk and M. Bloom, Physica 22, 555 (1966).

50. Ibid., p. 557.

51. T. Moriya, op. cit., p. 29.

52. J. A. Casey, private communication.

53. V. Jaccarino, Magnetism (G. J. Rado and H. Suhl, eds., Academic Press, Inc., New York, 1963), Vol. IIA, p. 325.

54. R. D. Spence, private communication.

APPENDICES

APPENDIX A

DETECTION OF FREE INDUCTION DECAY AND SPIN ECHO SIGNALS

Consider a cylindrical receiver coil of circular cross-section with diameter d, having n turns, oriented with its axis in the x-y plane, say along the y-axis. The coil is connected in parallel to a tunable capacitor C_t (see Fig. 3.10). Assume that a 90° pulse of H_1 has just been applied so that M, the magnetization originally in the z-direction, is now precessing in the x-y plane as shown in Fig. 2.1c. Assume further that the phase of the precession is such that

$$M_y = M \cos \omega_L t \tag{A.1}$$

where ω_L is the Larmor precession frequency. The magnetic induction B_y accompanying M_y is

$$B_y = 4\pi M_y = 4\pi M \cos \omega_L t \tag{A.2}$$

The magnetic flux through the coil is then

$$\phi = B_y A_{effective} = (4\pi M \cos \omega_L t)\zeta \frac{\pi d^2}{4} n \tag{A.3}$$

Where ζ, called the "filling factor" denotes the fraction of coil volume which is occupied by the sample. Letting $K = \pi^2 d^2 n\zeta$, and using Faraday's law, the induced emf is given by

$$\varepsilon = \frac{-d\phi}{dt} = K\omega_L M \sin \omega_L t \tag{A.4}$$

If C_t is tuned so that the tank circuit has a resonance frequency ω_L, the voltage across the coil is given by

$$V = Q\varepsilon = QK\omega_L M \sin \omega_L t = (A') \sin \omega_L t \qquad (A.5)$$

where $Q = \frac{Lcoil\ \omega_L}{Rcoil}$. This is an rf voltage of frequency ω_L. Note that A' is proportional to the filling factor ζ and to M, the magnitude of the z-component of magnetization just before the 90° pulse. As discussed in Chapter II, this voltage decays to zero because the individual moments, which make up M, get out of phase.

APPENDIX B

DERIVATION OF EXPRESSIONS FOR T_{1n} AND $M_z(t)$

Consider a system of spin 1/2 nuclei in a magnetic field $\underline{H}$ along the z-axis. Let N^+ be the number of nuclei in the state $m = +\frac{1}{2}$ and let N^- be the number of nuclei in the state $m = -\frac{1}{2}$. Then N, the total number of spins is given by

$$N = N^+ + N^- \tag{B.1}$$

Define n by

$$n = N^+ - N^- \tag{B.2}$$

The nuclear magnetization M is therefore proportional to n. Now

$$\frac{dN^+}{dt} = N^-W\downarrow - N^+W\uparrow = -\frac{dN^-}{dt} \tag{B.3}$$

where $W\uparrow$ denotes the probability per second that the coupling which produces spin-lattice relaxation will induce a transition upward in energy. Similarly W denotes the probability per second that the coupling will induce a downward transition. At thermal equilibrium, with $dN^+/dt = 0$, we get using (B.3)

$$\frac{N^-}{N^+} = \frac{W\uparrow}{W\downarrow} \tag{B.4}$$

where $W\uparrow$ and $W\downarrow$ are not equal because of the coupling between the nuclear spins and the lattice. Now from (B.1) and (B.2),

$$\begin{aligned} N^+ &= (\tfrac{1}{2})(N + n) \\ N^- &= (\tfrac{1}{2})(N - n) \end{aligned} \tag{B.5}$$

Using (B.2), (B.4) and (B.5) we can derive an expression for the population difference at thermal equilibrium. This is

$$n_o = N\left(\frac{W\downarrow - W\uparrow}{W\downarrow + W\uparrow}\right) \tag{B.6}$$

using (B.3) and (B.5) we find

$$\frac{dn}{dt} = N(W\downarrow - W\uparrow) - n(W\downarrow + W\uparrow) \tag{B.7}$$

and using (B.6)

$$\frac{dn}{dt} = (n_o - n)(W\downarrow + W\uparrow) \tag{B.8}$$

The solution of this equation is

$$n = n_o - ce^{-(W\downarrow + W\uparrow)t} \tag{B.9}$$

where c is determined by the initial conditions. Thus the approach to equilibrium is exponential with a characteristic time

$$T_{1n} = \frac{1}{W\uparrow + W\downarrow} \tag{B.10}$$

From Eq. (1.5) and (B.4)

$$\frac{W\uparrow}{W\downarrow} = e^{\gamma\hbar H/k_B T} \tag{B.11}$$

We generally consider temperatures such that $k_B T >> \gamma\hbar H$, so that $W\uparrow \simeq W\downarrow$. Therefore we can write

$$T_{1n} = \frac{1}{2W\downarrow} \tag{B.12}$$

without much error.

Recall that M_z is proportional to n. Therefore

$$M_z = M_o - c'e^{-t/T_{1n}} \qquad (B.13)$$

Applying (B.13) to the situation depicted in Fig. 2-1C, where $\underline{M}$ has been rotated 90° about $\underline{H}_1$ and now lies in the x-y plane, we have

$$M_z = M_o\,(1-e^{-t/T_{1n}}) \qquad (B.14)$$

Since when t = 0, M_z = 0 and from (B.13), c' = M_o.

APPENDIX C

DERIVATION OF MAGNON DENSITY OF STATES

The density of magnon states $\rho(E\alpha)$ is derived as follows. Let $\rho(E\alpha)dE$ be the number of states in energy range dE at E for k_o in solid angle $d\Omega$. This is the same as the number of states in range dk at k_o for k_o in $d\Omega$, which we represent by $C(k_o)dk_o$. So

$$\rho(E\alpha)dE = C(k_o)dk_o = C(k_o)\left(\frac{\partial \underline{k}}{\partial E}\right)_{\underline{k}_o} dE \qquad (C.1)$$

Now

$$C(k_o)dk_o = \frac{V}{8\pi^3}k_o^2 \sin\theta \, d\phi d\theta dk_o \qquad (C.2)$$

so

$$C(k_o) = \frac{V}{8\pi^3}k_o^2 d\Omega \qquad (C.3)$$

Therefore

$$\rho(E\alpha)dE = \frac{V}{8\pi^3}f(\underline{k}_o, p_o)k_o^2 d\Omega \qquad (C.4)$$

where

$$f(\underline{k},p) = \left|\frac{\partial E_{kp}}{\partial \underline{k}}\right|^{-1} \qquad (C.5)$$

APPENDIX D

LIST OF DATA FOR T_{1n} VS. T FOR H^1, Cl^{35}, Rb^{85}, AND Rb^{87}

DATA FOR H^1

T(°K)	T_1 (sec)	Date	T(°K)	T_1 (sec)	Date
1.286	3.65×10^{-4}	5/12/67	0.550	3.20×10^{-2}	5/13/67
1.285	3.90×10^{-4}	"	0.550	2.95×10^{-2}	"
1.170	5.80×10^{-4}	"	0.550	3.10×10^{-2}	"
1.170	6.40×10^{-4}	"	0.550	3.00×10^{-2}	"
1.010	9.60×10^{-4}	"	0.520	3.65×10^{-2}	"
1.010	1.13×10^{-3}	"	0.520	4.00×10^{-2}	"
0.835	2.85×10^{-3}	"	0.500	4.00×10^{-2}	"
0.835	3.10×10^{-3}	"			
0.835	3.50×10^{-3}	"			
0.765	4.30×10^{-3}	"			
0.765	4.80×10^{-3}	"			
0.680	1.08×10^{-2}	"			
0.680	1.07×10^{-2}	"			
1.225	5.35×10^{-4}	5/13/67			
1.100	9.80×10^{-4}	"			
1.110	8.00×10^{-4}	"			
0.725	8.30×10^{-3}	"			
0.725	7.00×10^{-3}	"			
0.725	7.10×10^{-3}	"			
0.600	1.92×10^{-2}	"			
0.590	2.00×10^{-2}	"			
0.550	2.80×10^{-2}	"			

DATA FOR Cl^{35}

T(°K)	T_1 (sec)	Date	T(°K)	T_1 (sec)	Date
1.280	1.05×10^{-3}	2/ 6/67	0.885	5.70×10^{-3}	2/10/67
1.280	8.50×10^{-4}	"	0.790	9.20×10^{-3}	"
1.010	3.20×10^{-3}	"	0.780	1.50×10^{-2}	"
1.001	3.40×10^{-3}	"	0.768	1.40×10^{-2}	"
0.865	6.40×10^{-3}	"	0.750	1.50×10^{-2}	"
0.845	7.20×10^{-3}	"	0.727	2.00×10^{-2}	"
0.705	2.00×10^{-2}	"	0.707	2.10×10^{-2}	"
0.700	1.80×10^{-2}	"	0.668	2.50×10^{-2}	"
0.637	2.60×10^{-2}	"	0.617	4.10×10^{-2}	"
0.645	2.60×10^{-2}	"	0.617	4.50×10^{-2}	"
0.600	3.40×10^{-2}	"	0.585	5.40×10^{-2}	"
0.605	3.40×10^{-2}	"	0.541	1.08×10^{-1}	"
0.550	5.70×10^{-2}	"	0.550	9.00×10^{-2}	"
0.550	6.00×10^{-2}	"	0.502	2.00×10^{-1}	"
0.503	1.80×10^{-1}	"	0.502	2.00×10^{-1}	"
1.140	1.40×10^{-3}	2/10/67			
1.140	1.35×10^{-3}	"			
1.055	2.20×10^{-3}	"			
1.055	2.20×10^{-3}	"			
0.980	3.38×10^{-3}	"			
0.980	3.30×10^{-3}	"			
0.885	5.20×10^{-3}	"			
0.885	6.00×10^{-3}	"			
0.885	5.00×10^{-3}	"			

DATA FOR Rb^{85}

T(°K)	T_1 (sec)	Date	T(°K)	T_1 (sec)	Date
1.042	1.53×10^{-2}	3/10/67	0.492	7.85×10^{-1}	3/10/67
0.992	2.17×10^{-2}	"	0.473	$1.00 \times 10^{+0}$	"
0.973	1.82×10^{-2}	"			
0.934	2.20×10^{-2}	"			
0.933	2.50×10^{-2}	"			
0.879	2.40×10^{-2}	"			
0.879	3.80×10^{-2}	"			
0.887	3.50×10^{-2}	"			
0.806	4.40×10^{-2}	"			
0.806	4.80×10^{-2}	"			
0.764	6.20×10^{-2}	"			
0.764	6.50×10^{-2}	"			
0.730	7.50×10^{-2}	"			
0.730	8.40×10^{-2}	"			
0.680	1.16×10^{-1}	"			
0.680	1.22×10^{-1}	"			
0.640	1.65×10^{-1}	"			
0.610	1.75×10^{-1}	"			
0.610	2.10×10^{-1}	"			
0.616	1.90×10^{-1}	"			
0.585	2.72×10^{-1}	"			
0.555	3.30×10^{-1}	"			
0.525	4.30×10^{-1}	"			
0.503	7.30×10^{-1}	"			
0.503	7.70×10^{-1}	"			

DATA FOR Rb^{87}

T(°K)	T_1 (sec)	Date	T(°K)	T_1 (sec)	Date
1.317	7.80×10^{-4}	5/05/67	0.800	1.00×10^{-2}	3/07/67
1.317	6.80×10^{-4}	"	0.787	1.06×10^{-2}	"
1.317	7.40×10^{-4}	"	0.787	1.08×10^{-2}	"
1.224	1.14×10^{-3}	"	0.738	1.30×10^{-2}	"
1.224	1.02×10^{-3}	"	0.727	1.76×10^{-2}	"
0.842	7.20×10^{-3}	4/25/67	0.646	2.60×10^{-2}	"
0.912	5.00×10^{-3}	"	0.617	3.30×10^{-2}	"
0.912	4.80×10^{-3}	"	0.577	5.70×10^{-2}	"
0.724	1.80×10^{-2}	"	0.587	5.20×10^{-2}	"
0.707	1.95×10^{-2}	"	0.552	7.00×10^{-2}	"
0.572	4.40×10^{-2}	"	0.550	7.00×10^{-2}	"
0.538	8.80×10^{-2}	"	0.517	1.23×10^{-1}	"
0.532	9.20×10^{-2}	"	0.509	1.23×10^{-1}	"
1.030	2.80×10^{-3}	3/07/67	0.488	1.70×10^{-1}	"
1.030	2.20×10^{-3}	"	0.450	4.60×10^{-1}	"
1.030	3.00×10^{-3}	"	0.432	5.20×10^{-1}	"
1.030	3.05×10^{-3}	"	1.296	9.40×10^{-4}	4/28/67
0.975	3.10×10^{-3}	"	1.320	9.70×10^{-4}	"
0.975	3.20×10^{-3}	"	1.497	6.00×10^{-4}	"
0.975	3.40×10^{-3}	"	1.220	1.07×10^{-3}	"
0.920	5.60×10^{-3}	"	1.258	1.10×10^{-3}	"
0.920	5.40×10^{-3}	"	1.258	1.04×10^{-3}	"
0.881	8.50×10^{-3}	"	1.258	1.03×10^{-3}	"
0.881	6.00×10^{-3}	"	1.258	1.07×10^{-3}	"

DATA FOR Rb^{87}

T(°K)	T_1 (sec)	Date
1.286	9.00×10^{-4}	4/28/67
1.210	1.42×10^{-3}	"
1.596	4.00×10^{-4}	4/05/67
0.035	2.70×10^{0}	6/14/67
0.032	4.50×10^{0}	"